Agricultural Water Management 333 (2026) 110538

Contents lists available at ScienceDirect

Agricultural Water Management

journal homepage: www.elsevier.com/locate/agwat

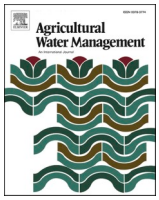

Climate impacts on agricultural water use revealed by multi-cropping irrigation dynamics in the Poyang Lake basin

Qianya Yang [a,b,*], Jianhui Wei [c,**], Chuanguo Yang [b], Huanghe Gu [b], Jianyong Ma [c], Ningpeng Dong [d], Lifeng Wu [a], Zhongbo Yu [b]

[a] School of Soil and Water Conservation, Jiangxi University of Water Resources and Electric Power, Nanchang, China
[b] The National Key Laboratory of Water Disaster Prevention, Hohai University, Nanjing, China
[c] Institute of Meteorology and Climate Research (IMKIFU), Karlsruhe Institute of Technology, Campus Alpin, Garmisch-Partenkirchen, Germany
[d] State Key Laboratory of Simulation and Regulation of Water Cycle in River Basin, China Institute of Water Resources and Hydropower Research, Beijing, China

ARTICLE INFO

Keywords:
Multi-cropping irrigation
Process-based modeling
Catchment hydrology
Climate change scenarios
Irrigation intensification scenarios
Compound extreme analysis

ABSTRACT

Future climate change is expected to modify the magnitude and timing of agricultural irrigation demand, but the mechanisms remain uncertain in humid monsoon regions where increased precipitation may offset warming-induced evapotranspiration. This study assesses future irrigation water use (IWU) over the Poyang Lake basin, China, using a previously developed NOAH-HMS land surface–hydrological model coupled with a crop-specific irrigation (CDI) scheme that distinguishes paddy rice and non-rice crops. Simulations are driven by bias-corrected CORDEX–East Asia climate projections under RCP2.6 and RCP8.5 for the mid-century (2031–2060) and late-century (2065–2094) periods. Results show that basin-mean IWU decreases in most future scenarios by about 3%–9%, mainly because projected precipitation increases largely offset warming-enhanced evapotranspiration. However, this basin-scale decline conceals seasonal and spatial heterogeneity. Regional IWU exhibits a "summer decline–autumn increase" pattern, with reductions in July–August and increases in October–November. Although rice IWU decreases, its within-season rise during the growing period becomes steeper. Non-rice IWU remains concentrated in late autumn and shows stronger sensitivity to warming and drying. Precipitation–temperature quadrant analysis shows that IWU in Dry–Hot years is generally higher than in wetter states, with the strongest increase occurring in the mid-century. Precipitation remains the primary driver of interannual IWU variability, but temperature exerts increasing influence toward the late century. These results demonstrate that basin-mean IWU changes alone could underestimate future irrigation risks, emphasizing the need to consider seasonal redistribution, crop-specific responses, local hotspots, and compound extremes in agricultural water management.

1. Introduction

Since the Industrial Revolution, rising anthropogenic CO_2 emissions have driven global warming and intensified the spatiotemporal variability of precipitation (Tukimat et al., 2017), increasing the risks of floods and seasonal droughts. Irrigation demand is highly sensitive to climate variability (Schlenker et al., 2007), particularly precipitation and temperature, which jointly regulate soil moisture availability and atmospheric evaporative demand (Frederick and Major, 1997). As a result, climate change is likely to amplify the uneven distribution of irrigation water demand over time and space, with implications for agricultural water allocation and regional water security.

Irrigation plays a central role in sustaining global food production, but it is also one of the most intensive human interventions in the terrestrial water cycle. Rapid population growth and technological advancement have expanded irrigation areas worldwide (Nazemi and Wheater, 2015), contributing to a sharp increase in agricultural water use (Hanasaki et al., 2013; Leng and Tang, 2014; Wada et al., 2013; Hao et al., 2024). Recent global assessments further show that irrigation expansion can increase crop production while intensifying freshwater stress. Mehta et al. (2024) reported that the global area equipped for irrigation increased by 11% from 2000 to 2015, with more than half of

* Corresponding author at: School of Soil and Water Conservation, Jiangxi University of Water Resources and Electric Power, Nanchang, China.
** Corresponding author.
E-mail addresses: yangqy@juwp.edu.cn (Q. Yang), jianhui.wei@kit.edu (J. Wei).

https://doi.org/10.1016/j.agwat.2026.110538
Received 15 March 2026; Received in revised form 6 June 2026; Accepted 11 June 2026
Available online 15 June 2026

this expansion occurring in already water-stressed regions. Jägermeyr et al. (2017) also showed that a substantial fraction of global irrigation water use occurs at the expense of environmental flow requirements. These findings highlight the growing tension between food production, irrigation development, and freshwater sustainability. Under climate change, irrigation is therefore increasingly regarded as both an adaptation measure and a potential source of additional water stress. Sustainable irrigation expansion may contribute to agricultural adaptation when water storage and deficit-irrigation strategies are carefully considered (Rosa et al., 2020), but future irrigation withdrawals are still projected to increase in many agricultural regions under high-emission scenarios (Haile et al., 2024). These findings indicate that future irrigation risk should be assessed not only as a crop water demand problem, but also as a coupled climate–land–water management issue.

Extensive research has examined future irrigation water demand from hydrological, agricultural, and interdisciplinary perspectives. Most assessments are based on climate projections derived from the Coupled Model Intercomparison Project (CMIP) or high-resolution regional climate simulations produced within the Coordinated Regional Climate Downscaling Experiment (CORDEX) framework, driven by emission scenarios proposed by the Intergovernmental Panel on Climate Change (IPCC). Both conceptual approaches and process-based models have been widely applied to estimate irrigation water demand under future climate conditions (Döll and Siebert, 2002; Elgaali et al., 2007; Fischer et al., 2007; Wisser et al., 2010; Wada et al., 2013; Santikayasa et al., 2014; Uniyal and Dietrich, 2021; Nie et al., 2021). Many studies project increasing irrigation demand under warming, primarily due to enhanced evapotranspiration (Döll and Siebert, 2002; De Silva et al., 2007; Fischer et al., 2007; Thomas, 2008; Leng et al., 2013). However, growing evidence indicates strong regional contrasts. In some humid regions, projected increases in precipitation may partially or fully offset warming-induced evapotranspiration, leading to stable or even declining irrigation water demand (Yoo et al., 2012; Acharjee et al., 2017; Tukimat et al., 2017; Sun et al., 2018). These divergent projections underscore the importance of precipitation–temperature interactions and reveal substantial uncertainty in monsoon-dominated basins, where water availability is tightly linked to seasonal rainfall variability (Chen et al., 2024).

Although future irrigation water demand has been widely assessed, several issues remain insufficiently addressed in humid monsoon basins. Many assessments rely on irrigation quotas or simplified crop water-use schemes, and therefore provide limited representation of crop-specific irrigation processes. This limitation is relevant for rice-dominated agricultural regions, because paddy irrigation is regulated by field ponding, water-depth management, drainage and drying periods, and the substitution of rainfall for irrigation. By contrast, irrigation for non-rice crops is more directly triggered by root-zone soil moisture deficits. In humid regions, abundant annual precipitation may also mask seasonal water shortages. As a result, future irrigation risk cannot be fully understood from annual irrigation totals alone. Seasonal redistribution, spatially uneven responses, crop-specific behavior, and irrigation demand under compound dry–hot conditions need to be examined together.

The Poyang Lake basin (PLB) in southeastern China provides a suitable case for this analysis. The basin has abundant monsoonal precipitation, strong intra-annual rainfall variability, extensive paddy rice cultivation, and close lake–river hydrological connections. Agricultural water use in this region is therefore strongly affected by the seasonal match between rainfall, crop water demand, and irrigation management. Previous studies in the PLB have mainly estimated irrigation water use using irrigation quotas or statistical approaches (Liu et al., 2019), while process-based assessments of future climate impacts on crop-specific irrigation demand remain limited. It is still unclear how projected precipitation and temperature changes may alter the seasonal timing, spatial distribution, and crop composition of irrigation water use in this humid monsoon basin.

To address these gaps, this study extends the NOAH-HMS-CDI framework previously developed and validated for PLB by Yang et al. (2025) to assess future climate-driven changes in IWU under different climate scenarios. This framework couples a land surface–hydrological model with a crop-specific dynamic irrigation scheme, distinguishing paddy rice and non-rice irrigation. It enables the analysis of annual IWU changes, seasonal redistribution, crop-specific responses, spatial heterogeneity, and dry–hot sensitivity. The objectives of this study are to: (1) project future crop-specific IWU responses under different climate scenarios; (2) examine how precipitation and temperature changes reshape the seasonal timing, spatial distribution, and crop composition of IWU; and (3) assess irrigation sensitivity under compound dry–hot conditions and irrigation intensification scenarios, with implications for adaptive agricultural water management in humid monsoon basins.

2. Methods and data

In this section, we describe the irrigation-represented NOAH-HMS-CDI model, its configuration, and modeling strategy. Additionally, we describe the observational datasets, regional climate projections, methods, and metrics used for model evaluation and impact assessment.

To provide an overview of the technical framework of this study, Fig. 1 illustrates the integrated workflow linking climate forcing, land surface–hydrology–irrigation simulation, irrigation scenario design, and impact and attribution analyses. Specifically, candidate CORDEX-East Asia (CORDEX-EA) regional climate model datasets were first evaluated against observed meteorological records, and the most suitable dataset for PLB was selected as the future climate forcing. The selected CORDEX-EA dataset was then bias-corrected against observations using quantile mapping for precipitation and the delta method for temperature. The corrected climate forcings were subsequently used to drive the NOAH-HMS-CDI coupled model, which explicitly represents land surface–hydrological processes and distinguishes irrigation schemes for rice and non-rice crops. Based on the baseline irrigation area, multiple irrigation intensification scenarios (+5% and +10%) were constructed for the historical period (1986–2015) and two future periods (2031–2060 and 2065–2094). The model outputs were subsequently analyzed to quantify changes in IWU, seasonal characteristics, and compound dry-hot extremes, and to attribute the relative contributions of precipitation and temperature using linear regression and the P–T quadrant approach, ultimately providing management-oriented insights for adaptive irrigation strategies.

2.1. NOAH-HMS-CDI

In this study, the NOAH-HMS-CDI model, a land surface-hydrological model with a crop-specific dynamic irrigation scheme (Yang et al., 2025), is employed for agricultural climate impact assessment. NOAH-HMS (Wagner et al., 2016) is a two-way coupled land surface–hydrologic model and accounts for physical processes of water and energy balances in a ground-soil-vegetation continuum. The governing equations of the land surface model NOAH include the one-dimensional Richards equation for the vertical exchange of soil moisture, the diffusion equation for the vertical exchange of soil energy, and the balance equations for water and energy (Chen and Dudhia, 2001). Evapotranspiration in NOAH is represented as the sum of direct soil evaporation, plant transpiration, and canopy-interception evaporation. Potential evaporation is estimated from the surface energy balance using a Penman–Monteith-type formulation, and the actual evaporation and transpiration are constrained by vegetation cover, canopy resistance, intercepted canopy water, and root-zone soil moisture availability (Chen and Dudhia, 2001).

As for the hydrological modeling system HMS (Yu et al., 2006), it consists of the two-dimensional diffusive wave equation, the equilibrium-state Richards equation, and the two-dimensional Boussinesq equation for the horizontal movement of surface- and subsurface

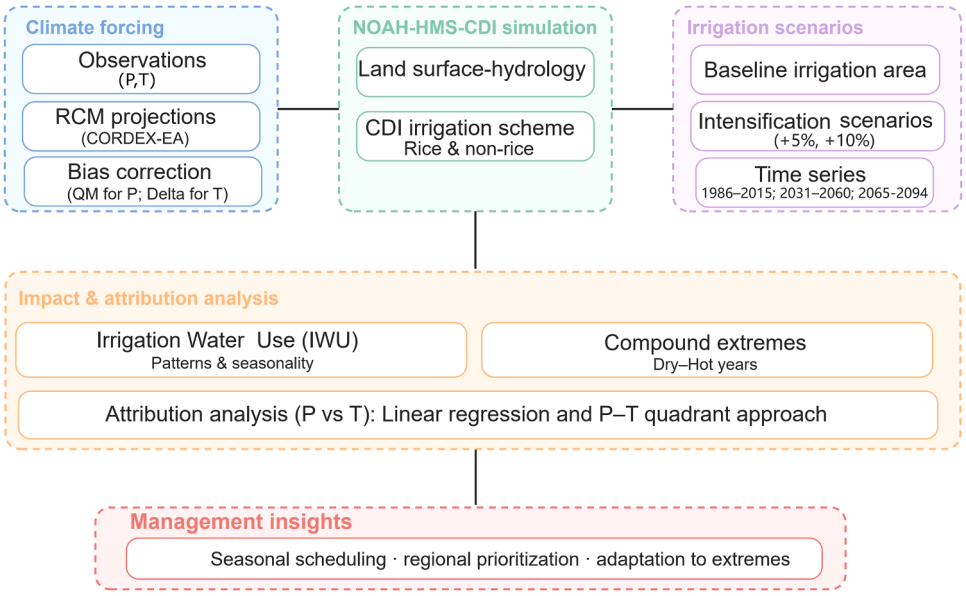

Fig. 1. Overall framework of the study integrating climate forcing, NOAH-HMS-CDI simulation, irrigation scenarios, and impact–attribution analyses.

water (Dong et al., 2022). In addition to the standalone mode of NOAH-HMS, NOAH-HMS can be fully coupled with the Weather Research and Forecasting model (Skamarock et al., 2008), enabling the potential of the joint atmosphere–hydrology modeling (Wagner et al., 2016).

To represent irrigation practices in NOAH-HMS, a crop-specific dynamic irrigation (CDI) scheme described in Yang et al. (2025) is used. A key feature of the CDI scheme is its ability to differentiate irrigation practices for rice and non-rice crops (Fig. 2), which allows a more realistic estimation of IWU. For rice, the model calculates its irrigation water requirement by maintaining a specified ponded water depth in paddy fields. IWU for rice is estimated in the model by closely following the local irrigation activities, such as cropping season, irrigation period, and field drying period. Irrigation is applied when the remaining ponded water from the previous time step plus precipitation is insufficient to maintain the prescribed target water depth.

For non-rice crops, irrigation water requirement is calculated using a soil moisture deficit method. The model first identifies the irrigation

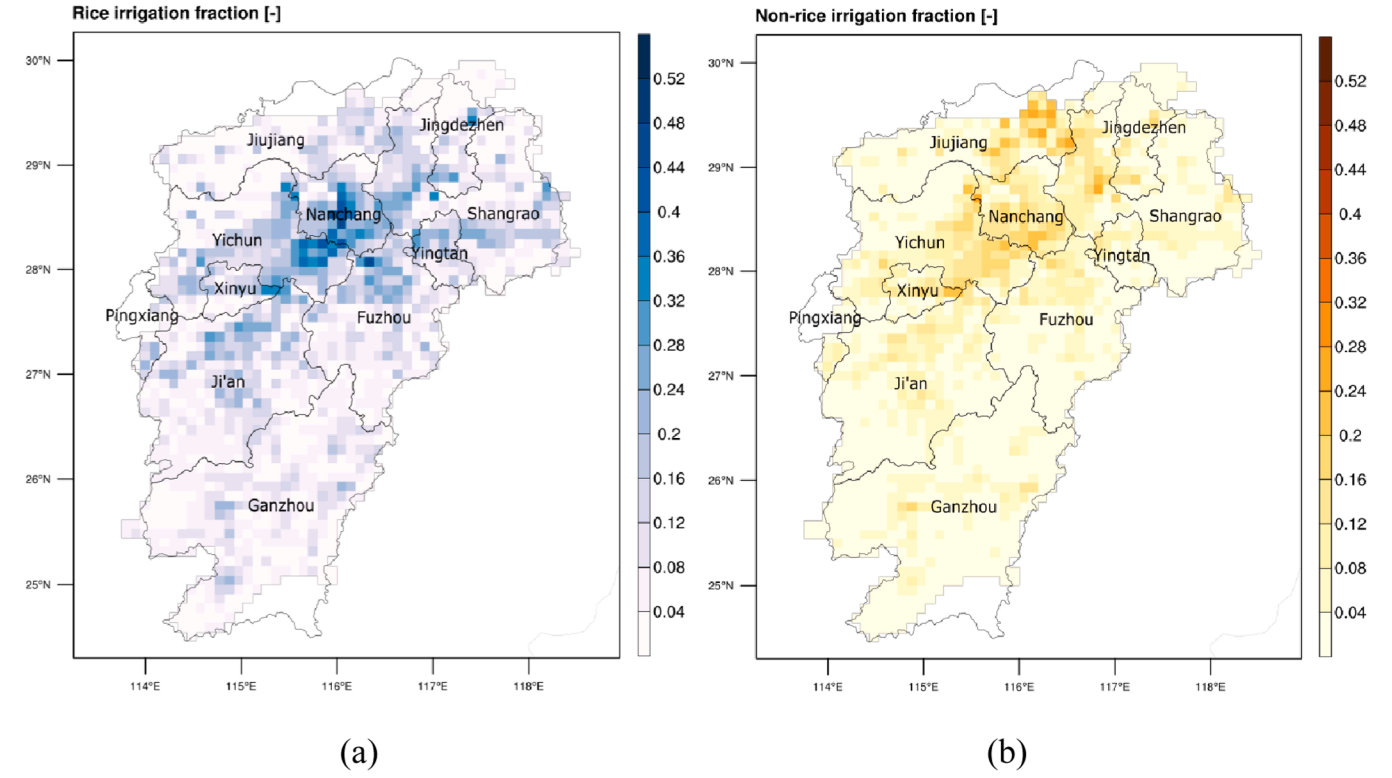

Fig. 2. Spatial distributions of the irrigation area fraction (–) at a horizontal resolution of 10 km × 10 km over PLB for (a) rice crops and (b) non-rice crops. The maps are derived from the Global Harvested Area and Yield (GHAYC) dataset covering 175 individual crop types. City boundaries within PLB are overlaid to show the locations of the main administrative areas.

period according to the greenness fraction. Irrigation is then triggered when crops are in the growing period and root-zone soil moisture availability falls below the prescribed threshold. Irrigation water requirement for non-rice crops is calculated as the amount of water required to raise the soil moisture at the root zone to its field capacity.

Irrigation water supply is represented through a virtual reservoir in NOAH-HMS. The virtual reservoir stores part of the surface runoff simulated by the model and releases water to meet crop-specific irrigation requirement. For rice, irrigation water is added to net precipitation to maintain the surface water layer over paddy fields. For non-rice crops, irrigation water is added to total precipitation as an additional water input to replenish root-zone soil moisture. A detailed description of the irrigation-represented NOAH-HMS model is given in Yang et al. (2025).

The coupling strategy among the land surface, terrestrial hydrology, and irrigation practices compartments is as follows: NOAH calculates surface runoff, subsurface runoff, and groundwater recharge, whereas HMS routes overland flow, channel flow, and subsurface flow. CDI retains part of the simulated surface runoff and then releases the stored water under crop-specific irrigation conditions. The updated surface water and soil moisture from CDI and HMS feed back into the processes of energy and water partitioning in NOAH, allowing the interactions across three compartments during the model iteration.

The irrigation-enabled NOAH-HMS-CDI framework has been previously evaluated over PLB under historical conditions (Yang et al., 2025), where it showed reasonable performance in reproducing the major hydrological processes and seasonal irrigation dynamics. On this basis, the model is applied here to assess future climate-driven changes in basin-scale hydrology and IWU.

2.2. Model configuration

In this study, we configure the irrigation-represented NOAH-HMS model for the multi-cropping PLB in Southeast China (Fig. 3). The PLB covers an area of about 162,200 km^2. The annual mean air temperature averaged over the basin is 17.5 °C and the precipitation is about 1640 mm year^{-1} (Wu et al., 2022). As the climate of the PLB is modulated by the East Asian summer monsoon, this region is known for its high spatial and temporal variability in precipitation (Zhang et al., 2011). Spatially, the precipitation amount within the basin is higher in its southeastern part than that in the northwestern part. Temporally, the rainy season lasts from April to June in association with the East Asian summer monsoon. The dry period covers November and December. It is reported that the wet-dry abrupt alternation in the PLB is strongly impacted by changes in the large-scale circulation patterns partly induced by El Niño-Southern Oscillations (Xing et al., 2022, 2024). Moreover, the interannual variability of precipitation in the basin is also high, which leads to drought and flood disasters there. For example, the precipitation amount in 2012 was nearly twice as high as that in 2011.

The basic NOAH-HMS model is configured for covering Southeast Asia including our study area PLB, with a spatial resolution of 10 km. This model configuration has been adopted in the recent studies of Wei et al. (2021) and Yang et al. (2025). Specifically, the land surface static inputs in NOAH consist of topography, soil properties, soil types and dominant land use derived from Food and Agriculture Organization of the United Nations (FAO) and United States Geological Survey (USGS). The hydrogeographic inputs in HMS, such as, hydraulic conductivity and river networks, are derived from the Chinese Geology data set and the USGS 1-km digital elevation data set (HYDRO1K). As for the configuration of the CDI scheme, the land-use types from USGS and the crop types from the Global Harvested Area and Yield for 175 Crops (GHAYC, Monfreda et al., 2008) are used.

The NOAH-HMS-CDI framework was previously evaluated over the Poyang Lake basin under historical conditions by Yang et al. (2025). The model was run for 2006–2015, with 2006 used as the spin-up period. Historical performance was evaluated using different observational datasets and periods: monthly streamflow at five hydrological stations for 2007–2015, 10-day topsoil moisture at three agrometeorological stations from August 2009 to July 2010, heat fluxes at the Qianyanzhou ChinaFLUX site for 2007–2010, and city-level annual irrigation water use records for 2007–2015.

For streamflow, the model captured the monthly variability well at the five stations, with correlation coefficients generally above 0.90;

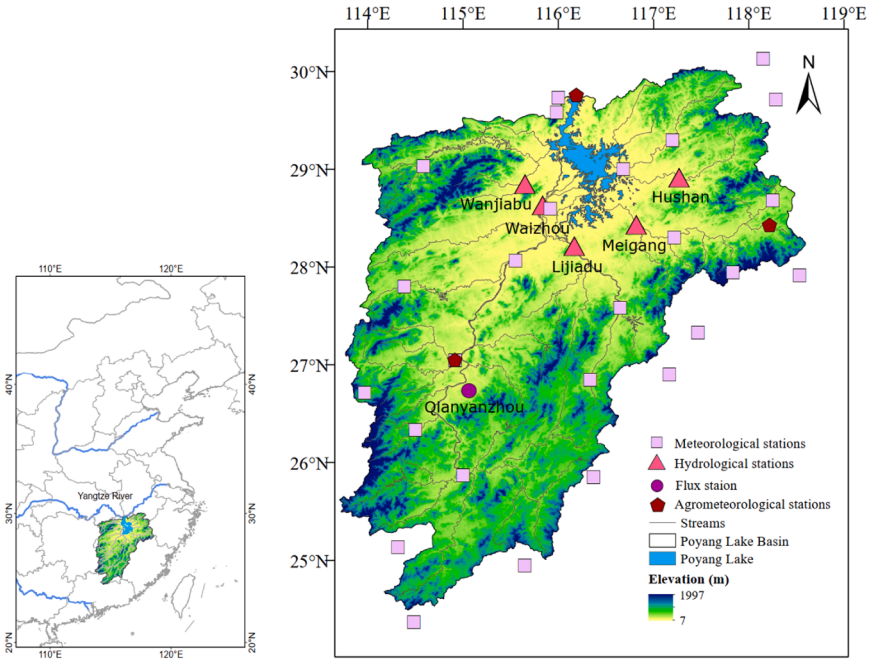

Fig. 3. Location of PLB. The left panel shows the location of PLB in China, situated in the middle reach of the Yangtze River basin; the right panel displays the elevation and river network of the basin, with rivers shown in gray. The pink squares, red triangles, purple circle, and dark red pentagons indicate the locations of meteorological stations, hydrological stations, the flux station, and agrometeorological stations, respectively.

better performance was found at Hushan and Waizhou, where NSE exceeded 0.85 and relative bias was within 10%. For soil moisture, the simulated top 10-cm soil moisture reproduced the observed wetting and drying variations at the three agrometeorological stations, with correlation coefficients above 0.70. The simulated heat fluxes also agreed reasonably with observations at Qianyanzhou, with correlation coefficients of 0.97 for latent heat flux and 0.80 for sensible heat flux. For IWU, the 10-km gridded simulations were aggregated to the city scale and compared with reported annual records. The CDI simulation reproduced the main spatial pattern of IWU. It slightly underestimated regional IWU, with a relative bias of −18% and a correlation coefficient of 0.72, but clearly outperformed the traditional dynamic irrigation scheme, which showed a relative bias of −57% and a correlation coefficient of 0.46. Groundwater recharge was analyzed as part of the simulated water budget, but groundwater was not independently validated because continuous and spatially representative groundwater observations are not available for the PLB.

2.3. Observed meteorological forcings

The time-varying observed meteorological forcing for the irrigation-enabled NOAH-HMS model is taken from station records. In the basin and its surrounding area, there are 26 meteorological stations operated by the National Meteorological Information Center of the China Meteorological Administration (Fig. 3). The station records encompass daily precipitation, 2-m air temperature, relative humidity, surface pressure, wind speed, surface downward longwave radiation, and surface downward solar radiation. For this study we collected the daily meteorological data for the years 1986–2015 from 26 stations, and spatially interpolated them to the 10 km grid using the bilinear interpolation method.

2.4. Selection of regional climate projections

To facilitate the climate impact assessment at the regional level, high-resolution climate projections are required to force the irrigation-enabled NOAH-HMS. In this study, the dynamically downscaled precipitation and 2-m air temperature are retrieved from Coordinated Regional Climate Downscaling Experiment for East Asia (CORDEX-EA). CORDEX was initiated by the World Climate Research Programme to support climate change, adaptation and vulnerability assessments, as well as government decision-making. CORDEX-EA provides a set of regional climate simulations driven by multiple emission scenarios from general circulation models.

The CORDEX-EA project consists of two phases: Phase I, with a horizontal resolution of 0.44° (~50 km), and Phase II, with a finer horizontal resolution of 0.22° (~25 km). In this study, we evaluate and assess the regional climate projections from both phases (Fig. S1 and S2), as numerous studies have demonstrated the added values of the dynamical downscaling in model evaluation (Park et al., 2013; Jin et al., 2016; Shen et al., 2017; Tang et al., 2017; P. Wang et al., 2019; E. Yu et al., 2015) and impact assessment (Hu et al., 2021).

We selected 11 GCM-RCM combinations (Tables 1 and 2) to evaluate their performance in reproducing historical (observed) regional climate over the PLB. The general circulation models of HadGEM2-AO, HadGEM2-ES, MPI-ESM-LR, and NorESM1-M are selected because of their superior performance in reproducing the climate of East Asia (Bao et al., 2014; Lee and Wang, 2014; Siew et al., 2014; Wang et al., 2015; Xu et al., 2017; Dong et al., 2020). Based on their performance in reproducing the observed climate over PLB, the dataset from HadGEM2-ES–RegCM4.4 is selected as the future climate forcing for the NOAH-HMS-CDI simulations (Fig. S1 and S2). Before being used to drive the NOAH-HMS-CDI simulations, the selected CORDEX-EA precipitation and 2-m air temperature are bias-corrected against observations. Daily precipitation is corrected using quantile mapping, and temperature using the delta method.

Table 1
Selected Models under the CORDEX-EA-I Framework.

CORDEX-EA-I					
GCM	HadGEM2-AO				
Number	1	2	3	4	5
RCM	HadGEM3-RA	RegCM4	MM5	WRF	RSM
Resolution	0.44°	50 km	50 km	50 km	50 km
Affiliation	MOHC	ICTP	NCAR	NCAR	YSU

2.5. Modeling strategy for irrigation impact analysis

In this study, the historical period of 1986–2015 is selected as the baseline to represent the modern hydroclimatic and irrigation conditions in the PLB. For the impact analysis, two future periods, 2031–2060 and 2065–2094, are considered to assess regional climate change and irrigation water use in the mid-century and late-century, respectively. Each period covers 30 years to ensure robust climate change signals and impact assessment, while minimizing the influence of interannual variability. It is worth noting that the NOAH-HMS-CDI modeling framework used here has been extensively validated and evaluated in our recent study of Yang et al. (2025) for 2007–2015. This study further expands the historical simulation period up to 30 years and sheds light on projected variations of irrigation water use under different climate change scenarios.

In order to further understand the resilience of the current (parameterized) irrigation practice (Section 2), we designed two intensified irrigation scenarios: (1) “FRA + 5%”, the GHAYC-based irrigated fraction (FRA) is increased by 5% relative to the baseline fraction (Fig. 2) and (2) “FRA + 10%”, the irrigated fraction is increased by 10%. Both scenarios were implemented for the two future periods, with particular focus on the high-emission RCP8.5 pathway.

Regarding the technical implications, the increases are applied only to model pixels classified as cropland and are proportional to the GHAYC-based irrigation area fraction (Fig. 2). In this study, we do not differentiate the irrigation intensification increases across crop types and sub-regions.

We closely follow Mehta et al. (2024) in selecting the degree of irrigation intensification. Their study reported that the global area equipped for irrigation (AEI) increased by 11% from 2000 to 2015. In addition, PLB was identified as a region with potential for sustainable AEI expansion (see Fig. 4a in Mehta et al., 2024). Under these circumstances, we developed irrigation intensification scenarios with increases of + 5% (moderate level) and + 10% (global average). These scenarios represent moderate and global average levels of potential AEI expansion within our multiple-cropping modeling system. It is worth noting that the designed scenarios here are consistent with China’s agricultural water policy reforms (Shah et al., 2023) and the well-facilitated farmland construction project (Wang et al., 2025), both of which aim to sustainably improve farmland-use efficiency.

2.6. Precipitation–temperature (P–T) quadrant analysis

To investigate the combined effects of precipitation and temperature on IWU under compound hydroclimatic conditions, a precipitation–temperature (P–T) quadrant analysis was employed. Annual basin-averaged precipitation and 2-m air temperature were first calculated. The 20th and 80th percentiles of the annual precipitation and temperature during the historical baseline period were then used as fixed reference thresholds and applied consistently to both the historical and future simulations. Based on the historical thresholds, each year in the historical and future simulations was classified into one of four compound hydroclimatic states: Wet–Cold ($P \geq P80$ and $T \leq T20$), Wet–Hot ($P \geq P80$ and $T \geq T80$), Dry–Cold ($P \leq P20$ and $T \leq T20$), and

Table 2
Selected Models under the CORDEX-EA-II Framework.

CORDEX-EA-II						
GCM	HadGEM2-ES		MPI-ESM-LR		NorESM1-M	
Number	6	7	8	9	10	11
RCM	REMO2015	RegCM4.4	REMO2015	RegCM4.4	REMO2015	RegCM4.4
Resolution	0.22°	25 km	0.22°	25 km	0.22°	25 km
Affiliation	MOHC	MOHC	MPI-M	MPI-M	NCC	NCC

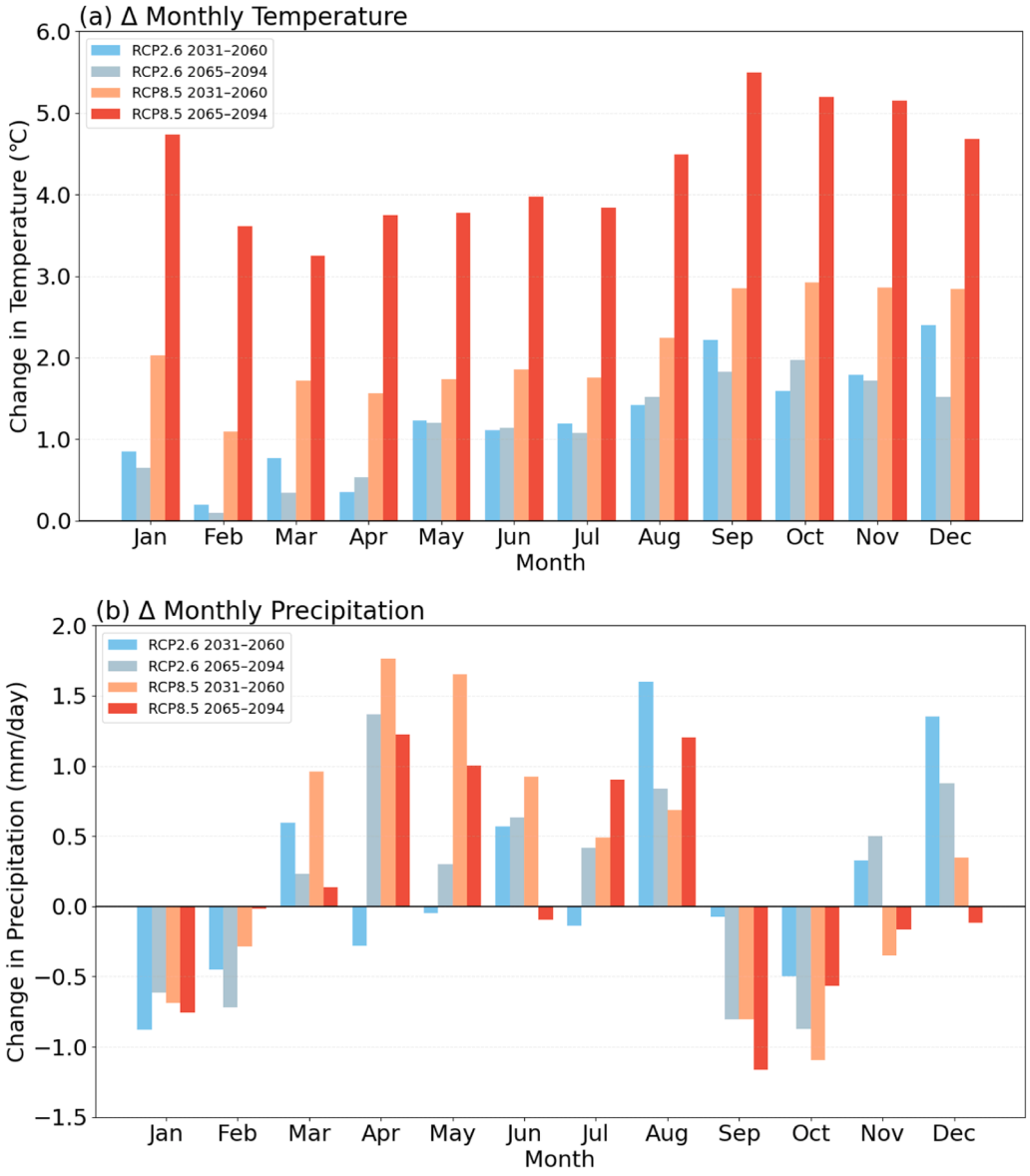

Fig. 4. The basin-averaged monthly changes in (a) temperature (°C), temporally averaged for 30 years. The changes are derived by comparing the mid-century (2031–2060) and late-century (2065–2094) simulations to the historical baseline (1986–2015), under the RCP2.6 and RCP8.5 climate scenarios. (b) as in (a) but for simulated precipitation changes in PLB (mm/day).

Dry–Hot (P ≤ P20 and T ≥ T80), where P20/P80 and T20/T80 denote the 20th and 80th percentiles of precipitation and temperature, respectively.

For each hydroclimatic state, the corresponding annual basin-averaged IWU was extracted for all classified years. The mean IWU of each state was then calculated. To quantify the amplification effect of compound warm–dry conditions, the relative differences in mean IWU between Dry–Hot (DH) years and each of the other three hydroclimatic states were computed as

$$\Delta IWU_{DH-X} = \frac{\Delta IWU_{DH} - \Delta IWU_X}{\Delta IWU_X} \times 100\%$$

where X denotes Wet–Cold, Wet–Hot, or Dry–Cold conditions. This metric provides a normalized measure of the sensitivity of IWU to compound precipitation–temperature extremes, enabling a systematic diagnosis of climate–irrigation interactions beyond univariate analyses

of precipitation or temperature alone.

2.7. Climatic attribution analysis

The relative contributions of precipitation and temperature to interannual variations in IWU are quantified using standardized multiple linear regression at the annual scale. Basin-averaged annual IWU is regressed against annual precipitation and mean temperature after standardizing all variables to remove unit effects. The relative contribution of each climatic factor is calculated from the normalized absolute values of the standardized regression coefficients, representing their relative explanatory power within the linear framework.

3. Results

3.1. Projected changes in temperature and precipitation

In this section, we present the projected temperature and precipitation changes for the mid-century (2031–2060) and late-century (2065–2094) periods under RCP2.6 and RCP8.5.

Basin-mean annual temperature increases by approximately 1.1–1.3 °C under RCP2.6 and by about 2.1 °C (mid-century) and 4.3 °C (late-century) under RCP8.5, relative to the historical baseline (1986–2015; Fig. 4a). The warming signal is spatially coherent across the basin, with larger increases occurring in the northern and northwestern regions, particularly around Jiujiang (Fig. S4).

In contrast, projected precipitation changes are smaller in magnitude but exhibit pronounced seasonal and spatial heterogeneity. Basin-mean precipitation increases by approximately 3–7% in the mid-century and remains positive in the late-century under both scenarios (Fig. 4b). However, this overall wetting masks a clear intra-annual redistribution, with increased precipitation mainly in spring and summer and drying tendencies emerging in early autumn, especially during September–October under RCP8.5. Spatially, precipitation increases are strongest in the central–eastern basin (e.g., Fuzhou), while northern and southwestern regions experience weaker increases or slight decreases (Fig. S3).

3.2. Responses of soil moisture and evapotranspiration

In this section, we examine the climate change-induced variations in basin-averaged 1-meter soil moisture and evapotranspiration, derived from the NOAH-HMS-CDI simulations.

The simulated top 1-meter soil moisture and evapotranspiration (ET) respond coherently to the projected climate changes. Basin-averaged 1-meter soil moisture generally decreases in winter and late autumn, but increases in late summer, especially around August-September. During the crop growing season (April–October), changes in mean soil moisture

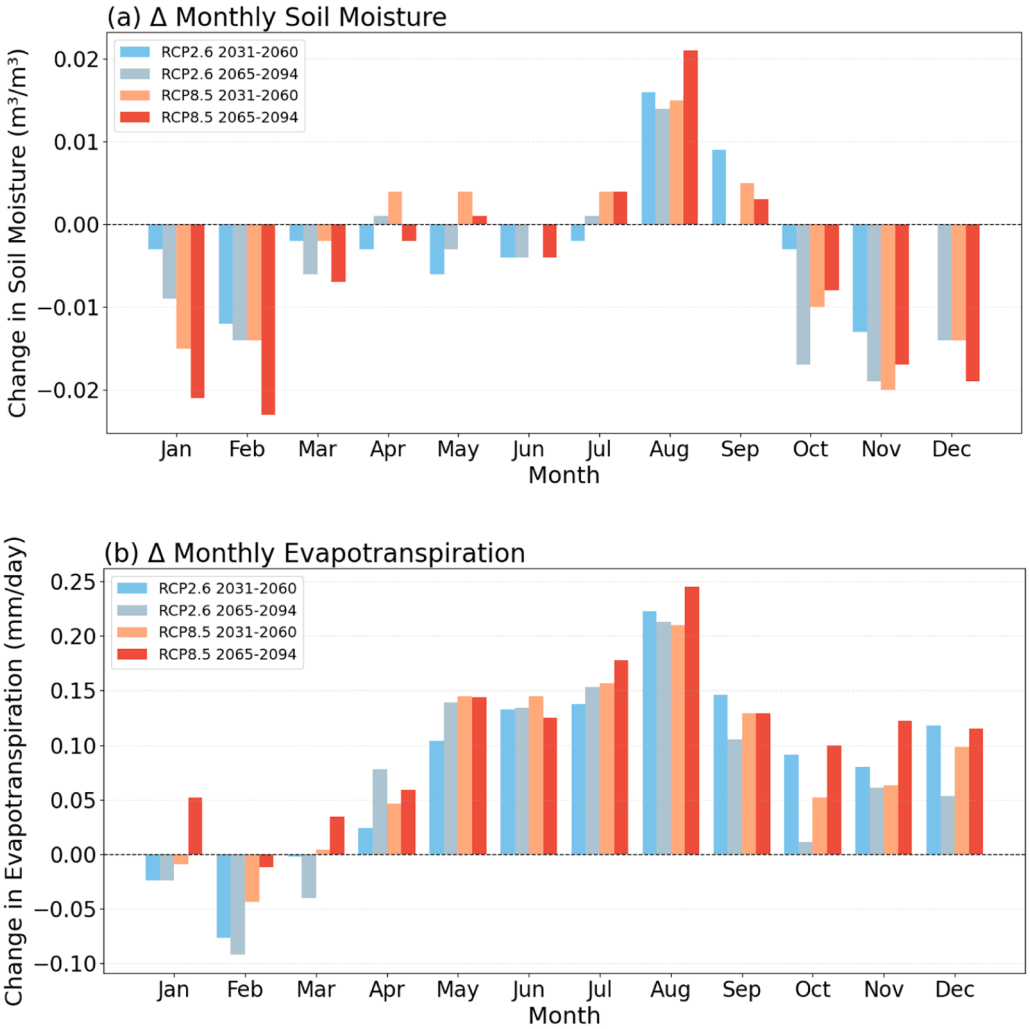

Fig. 5. The basin-averaged monthly changes in (a) the simulated top 1-meter soil moisture (m^3/m^3), temporally averaged for 30 years. The changes are derived by comparing the mid-century (2031–2060) and late-century (2065–2094) simulations to the historical baseline (1986–2015), under the RCP2.6 and RCP8.5 climate scenarios. (b) as in (a) but for the simulated evapotranspiration (mm/day).

are relatively small (within ±1%), yet their seasonal contrast is pronounced, with wetter summers and drier autumns (Fig. 5a).

Evapotranspiration increases throughout most of the year in all future scenarios, particularly from May to September. Growing-season ET increases by approximately 4% in the mid-century and 4.7% in the late-century, with stronger enhancement under RCP8.5. These results indicate that warming-driven increases in atmospheric evaporative demand are partially compensated by enhanced precipitation in summer, but not during autumn when precipitation declines (Fig. 5b).

3.3. Basin-scale irrigation water use and seasonal redistribution

Despite enhanced evapotranspiration, basin-mean IWU decreases in most future scenarios. Relative to the historical period, IWU decreases by about 8.8% (RCP2.6) and 3.2% (RCP8.5) in the mid-century, and by 3.4% (RCP8.5) in the late century. A slight increase (1.35%) is simulated only for the late-century period under RCP2.6. These results suggest that increased precipitation generally offsets the warming-induced increase in IWU at the basin scale.

More pronounced changes occur in the intra-seasonal distribution of IWU. In all future scenarios, IWU decreases in mid-summer, especially in July and August, but generally increases in autumn, particularly in October and November. IWU in August decreases by up to 1.8 mm/month under mid-century RCP2.6 and late-century RCP8.5, whereas October IWU increases by more than 2.1 mm/month under late-century RCP2.6. This "summer decline–autumn rise" pattern reflects a shift in

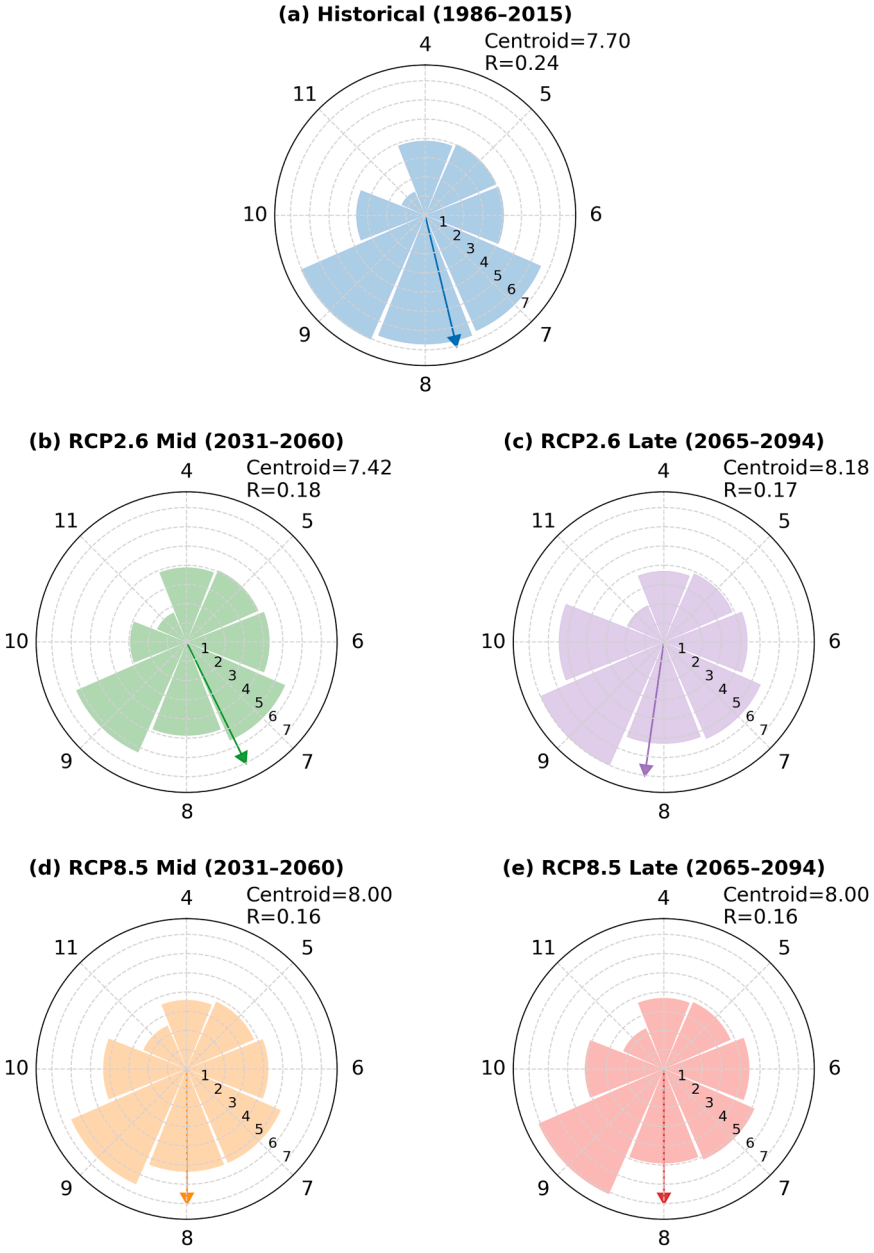

Fig. 6. (a) Centroid month (Apr–Nov) and concentration (R) of 30-year averaged monthly irrigation water use (IWU, mm/month) during the historical period (1986–2015). The outer ring represents months from April to November, and the radial distance denotes monthly IWU (mm/month), averaged for 30 years. The centroid indicates the weighted average timing of IWU within the irrigation season, and the concentration (R) quantifies how concentrated the irrigation is around the centroid month, with higher values indicating more focused irrigation and lower values indicating more evenly distributed irrigation over the season. (b, c) as in (a), but for IWU during the mid-century (2031–2060) and late-century (2065–2094) periods under RCP2.6 climate scenario, respectively. (d, e) as in (b, c), but for the RCP8.5 climate scenario.

the seasonal alignment between rainfall supply and irrigation water demand.

This redistribution is further summarized by the centroid analysis (Fig. 6). For each period and scenario, the temporal centroid was calculated from the 30-year averaged monthly IWU during April–November. The eight months were evenly assigned to a circular scale, and monthly IWU was used as the weight. The centroid month indicates the weighted timing of IWU within the irrigation season, while the vector length (R) indicates the degree of seasonal concentration. The centroid analysis shows that IWU tends to shift toward the later irrigation season. In most future scenarios, the centroid month moves from 7.7 to about 8–8.18, while R decreases from 0.24 to 0.16–0.18. This indicates a

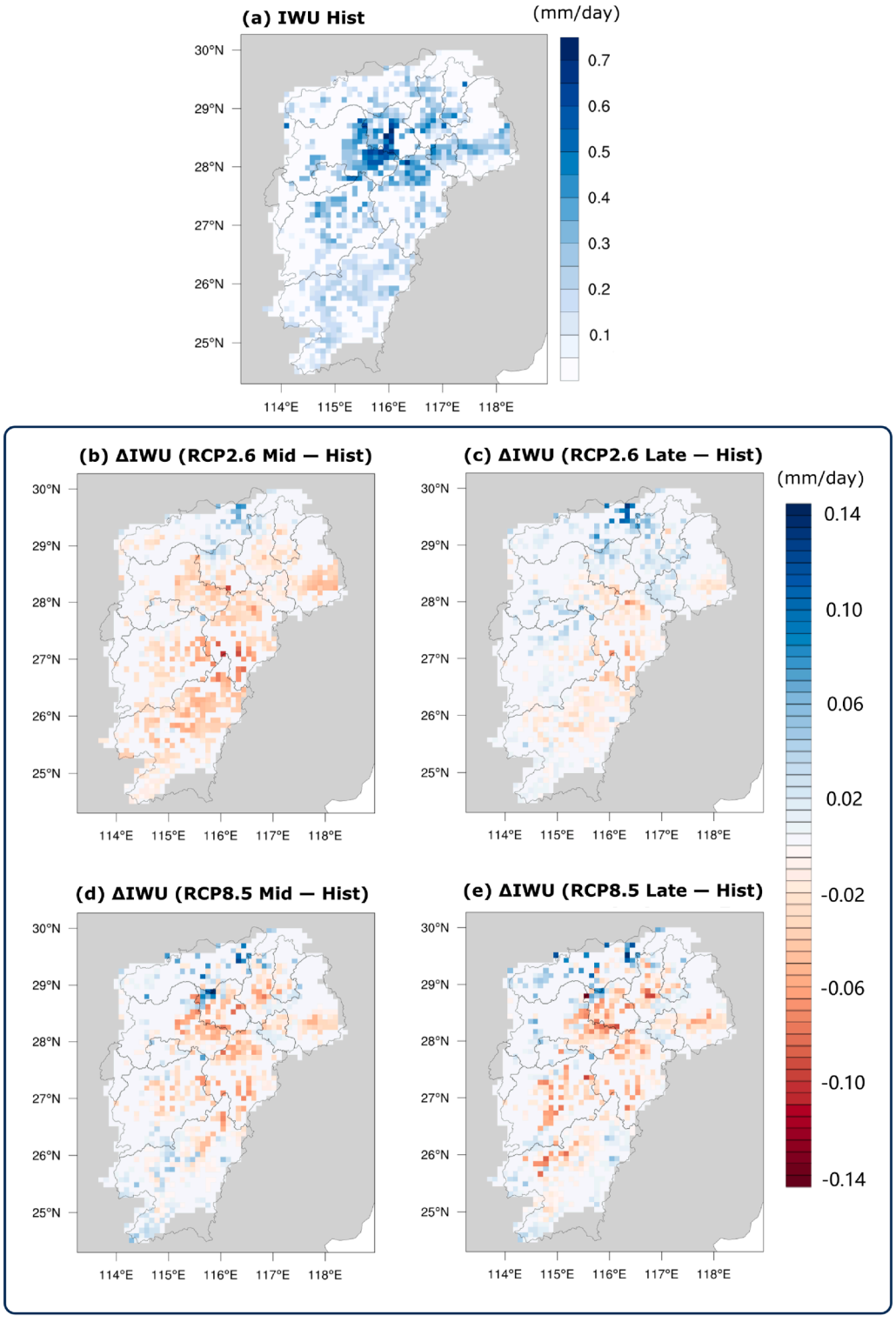

Fig. 7. (a) Spatial distribution of the 30-year averaged simulated irrigation water use (IWU in mm/day) over PLB, averaged for the historical period 1986–2015. (b) Spatial patterns of the differences in the simulated irrigation water use ΔIWU (mm/day) between the mid-century (2031–2060) simulation under RCP2.6 and the historical simulation. (c) as in (b), but for the differences ΔIWU between the late-century (2065–2094) simulation under RCP2.6 and the historical simulation. (d, e) as in (b, c), but for the differences ΔIWU under RCP8.5.

weaker summer concentration and a greater contribution of autumn IWU.

3.4. Spatial heterogeneity of irrigation responses

The basin-average decrease in IWU conceals strong spatial heterogeneity. Fig. 7 shows the spatial patterns of the 30-year averaged IWU derived from the historical (1986–2015) period and of the differences in the simulated IWU between the future periods and the historical (baseline) period. Most regions experience reduced IWU in the future, whereas northern parts of the basin show increased IWU (Fig. 7). City-level analysis reveals that Jiujiang is the only city exhibiting consistent increases in IWU in the mid-century under both scenarios (+10.7% under RCP2.6 and +18.8% under RCP8.5). In contrast, Fuzhou shows the largest reductions (−14.8% and −12.1%), corresponding to substantial projected precipitation increases (Fig. S3). In the late century, irrigation responses diverge further. Under RCP2.6, several cities experience increased IWU, while under RCP8.5 most cities show declining IWU, particularly in precipitation-enhanced regions such as Nanchang and Fuzhou (Fig. S3).

3.5. Crop-specific irrigation responses to climate change

Fig. 8 shows the monthly variations in the area-averaged irrigation water use for rice and non-rice crops, derived from the five simulations. From the perspective of crop type, rice irrigation exhibits a clear intra-annual rise, increasing from spring to late summer and peaking in September. From the historical to the mid- and late-century periods, the rice IWU curves show a more pronounced rise during the growing season, with a progressively steeper month-by-month increase within the year. This indicates that future climate change strengthens the within-season build-up of rice irrigation demand, although the total rice IWU

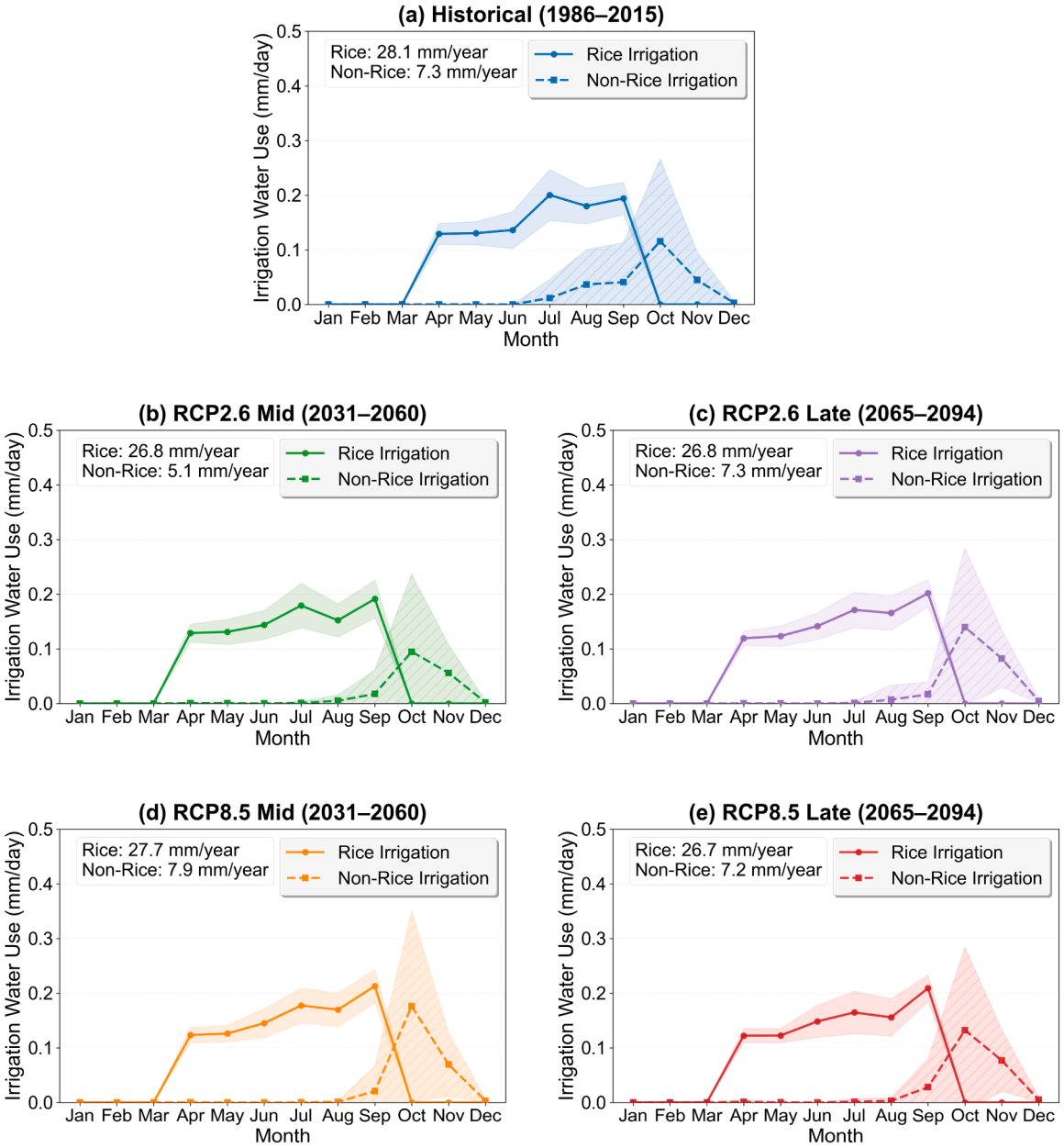

Fig. 8. (a) Monthly variations of the basin-averaged simulated irrigation water use (IWU in mm/day) for rice (solid line) and non-rice crops (dashed line), derived from the historical (1986–2015) simulation. Shaded areas represent the interannual variations of the monthly IWU. (b, c) as in (a), but derived from the mid-century simulation and the late-century simulation under RCP2.6, respectively. (d, e) as in (b, c) but derived from the simulations under RCP8.5.

generally decreases. In contrast, non-rice irrigation remains low for most of the year and is concentrated in pronounced late-season peaks in September–October. Moreover, non-rice irrigation is more responsive to emission scenarios in the mid-century period, with RCP8.5 showing larger increases than RCP2.6, whereas this scenario dependence becomes weaker in the late-century period (Fig. 8).

The contrasting irrigation trends between Fuzhou and Jiujiang further clarify the basin-wide patterns (Fig. S5 and S6). In Fuzhou, where total IWU decreases most in the mid-century, monthly IWU reveals a clear reduction in both rice and non-rice irrigation, particularly under RCP2.6, consistent with the projected increase in precipitation, which reduces IWU. By contrast, Jiujiang, the only city showing increasing total IWU under both RCP scenarios in the mid-century, exhibits relatively small intra-annual changes in rice irrigation, but with an overall increase in rice IWU. The increase is even more pronounced for non-rice irrigation, especially in autumn with the maximum increase reaching about 50%. This divergent behavior is consistent with the combined effects of pronounced warming and reduced precipitation in Jiujiang, which together enhance irrigation demand for both crop types.

3.6. City-level responses to irrigation intensification scenarios

Fig. 9 shows that under the RCP8.5 scenario, city-level changes in IWU under the no-intensification baseline and the intensified irrigation scenarios (+ 5% and + 10%) exhibit clear spatial differences relative to the historical period (1986–2015). The responses are generally stronger in the late-century (2065–2094) than in the mid-century (2031–2060). In addition, the + 10% scenario generally produces larger changes than the + 5% scenario, indicating that a greater increase in irrigation intensity leads to a stronger effect on regional IWU.

During 2031–2060, the responses vary considerably among cities, with both positive and negative changes observed. The largest increase occurs in Jiujiang, where IWU rises by about 0.009 and 0.012 mm/day under the + 5% and + 10% scenarios, respectively. IWU also increases noticeably in Nanchang, especially under the + 10% scenario, and shows slight increases in Ganzhou and Yingtan. In contrast, the largest decrease occurs in Fuzhou, where IWU declines by about 0.017 and 0.013 mm/day under the two scenarios. IWU also decreases in Ji'an, Shangrao, Xinyu, and Yichun, while changes in Jingdezhen and Poyang remain close to zero. These results indicate that in the mid-century, the effect of irrigation intensification on IWU does not follow a uniform pattern across cities.

By 2065–2094, city-level IWU changes are dominated by increases. Except for Fuzhou, IWU increases in all cities under both intensified irrigation scenarios. The largest increases occur in Jiujiang, Nanchang, and Yichun. In Jiujiang, IWU rises by about 0.017 and 0.019 mm/day under the + 5% and + 10% scenarios, respectively. The corresponding increases are about 0.008 and 0.016 mm/day in Nanchang, and about 0.008 and 0.018 mm/day in Yichun. IWU also increases in Ganzhou, Jingdezhen, Shangrao, Xinyu, Ji'an, and Yingtan, although with smaller

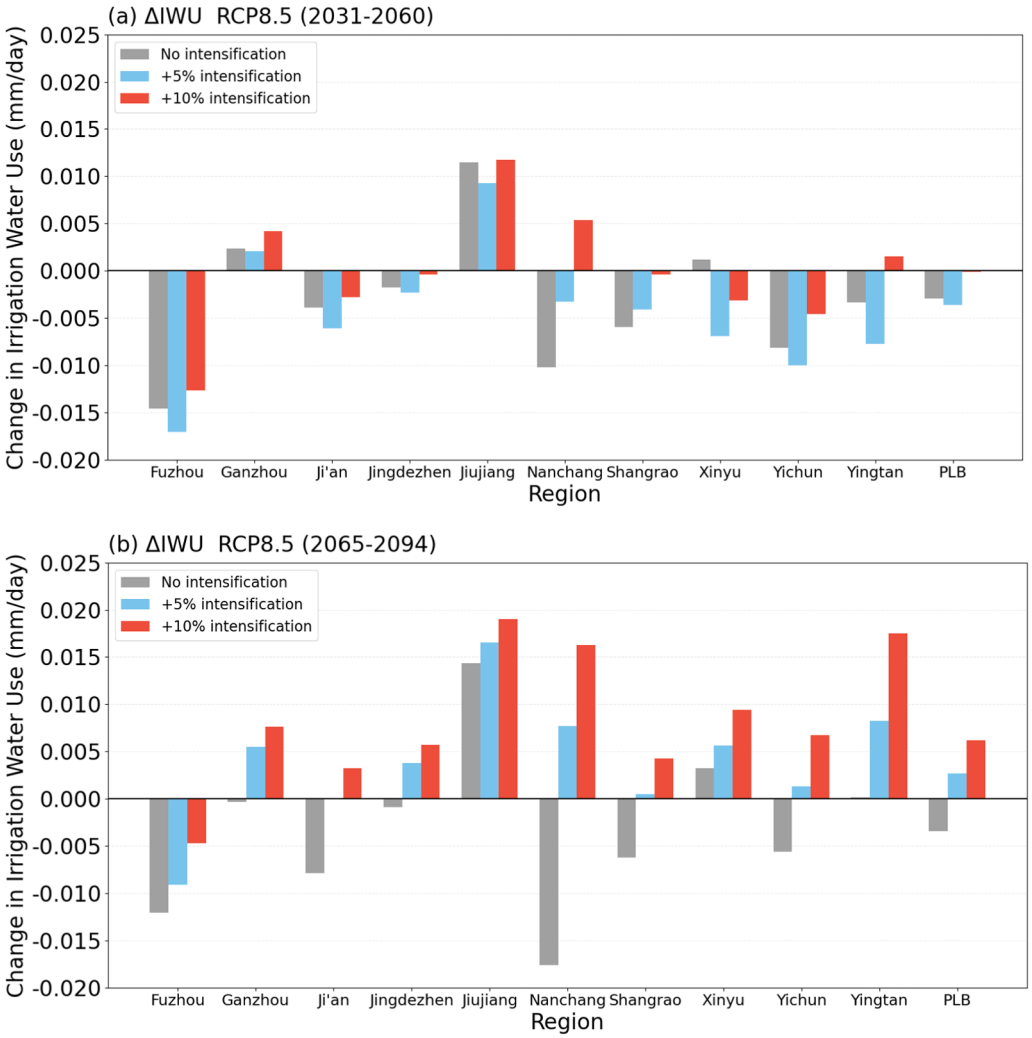

Fig. 9. City-level changes in IWU under RCP8.5 relative to 1986–2015 for 2031–2060 (a) and 2065–2094 (b) under the no intensification, + 5%, and + 10% irrigation intensification scenarios.

magnitudes. Fuzhou is the only city that still shows reduced IWU under the intensified scenarios, although the magnitude of decline is smaller than that in the mid-century. Overall, these results suggest that the effect of irrigation intensification on IWU becomes stronger over time and remains highly heterogeneous across the basin.

3.7. Climate–irrigation interaction and compound dry-hot effect

The P–T quadrant analysis is used to examine annual IWU under compound hydroclimatic conditions. For comparison, the 20th and 80th percentiles of annual precipitation and temperature derived from the historical period are used as thresholds to classify four types of extremes including "Dry-Hot", "Wet-Hot", "Dry-Cold", and "Wet-Cold". The defined thresholds are then applied to analyze all future projections under two scenarios to assess their impacts on the simulated IWU. Fig. 10 shows that climate change leads to consistently higher temperatures in the Poyang Lake basin across the investigated scenarios, but the projected precipitation change signals vary. As a result, two hot compound extremes ("Dry-Hot" and "Wet-Hot") are projected to occur more frequently, in comparison to those during the historical period (Fig. 10 and Table S1). Table 3 further quantifies the IWU contrast between Dry–Hot and Wet–Hot years. Under RCP2.6, the projected IWU is higher in Dry–Hot years than in Wet–Hot years in both future periods. The relative difference in IWU due to future drying is 27.2% in the mid-century period (a bootstrap-based 95% confidence interval of

Table 3
The relative differences in the projected IWU (%) between the identified Dry–Hot years and Wet–Hot years during three periods under two scenarios.

Scenario	Dry–Hot vs. Wet–Hot (%)	Bootstrap 95% CI
Historical (1986–2015)	13.2	Limited samples
RCP2.6 (2031–2060)	27.2	11.1–45.2
RCP2.6 (2065–2094)	16.2	−11.9–50.6
RCP8.5 (2031–2060)	33.6	Limited samples
RCP8.5 (2065–2094)	No Dry–Hot years	Not estimated

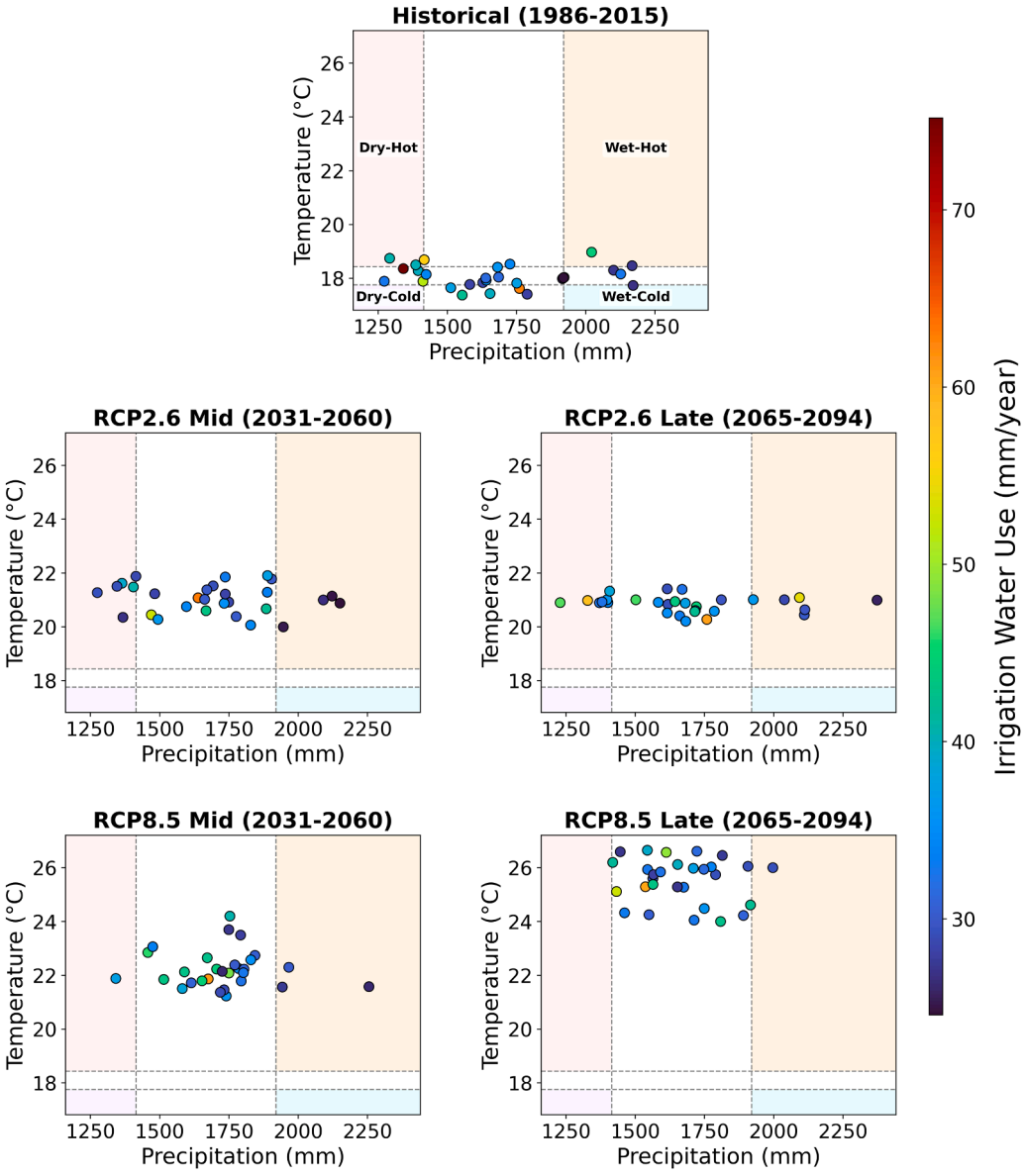

Fig. 10. Precipitation–temperature (P–T) quadrant classification with compound hydroclimatic state shading. The dashed lines represent the 20th and 80th percentile thresholds of annual precipitation and temperature derived from the historical period (1986–2015) and applied to future scenarios. Colored background regions denote Wet–Cold (cyan), Wet–Hot (orange), Dry–Cold (lavender), and Dry–Hot (red) conditions. Points represent individual years and are colored by IWU using a unified color scale across scenarios.

11.1–45.2%). Such drying-induced IWU difference becomes lower in the late-century period (16.2%) with a wider confidence interval (−11.9% to 50.6%). As for the RCP8.5 scenarios, a similarly large positive difference (33.6%) is found during the mid-century, but no confidence interval is estimated due to limited sample size.

3.8. Climate factor contributions

Fig. 11 shows the relative contributions of precipitation and temperature to interannual variations in IWU for the historical period and future climate scenarios. As shown in Fig. 11, precipitation is the dominant driver of IWU variability in all periods. During the historical period, precipitation accounts for 74% of the total variability, while temperature contributes 26%. Under RCP2.6, the contribution of precipitation decreases slightly from 70% in the mid-century period to 64% in the late-century period, accompanied by an increase in the temperature contribution from 30% to 36%. In contrast, RCP8.5 exhibits a different temporal pattern. In the mid-century period, precipitation explains 91% of IWU variability, with temperature contributing only 9%. By the late-century period, the contribution of precipitation decreases to 70%, while the temperature contribution increases to 30%.

4. Discussion

4.1. Climatic control on IWU in a humid monsoon basin

Basin-mean IWU generally decreases in most future scenarios despite projected warming, primarily due to enhanced precipitation (Section 3.1; Fig. 4) that offsets warming-induced increases in evapotranspiration. This reduction does not imply a weakened climatic influence; rather, it reflects the dominant role of precipitation in regulating soil moisture availability in humid monsoon systems (Chen et al., 2023). Under irrigation schemes triggered by root-zone soil moisture deficits, increases or improvements in the seasonal distribution of rainfall can substantially reduce irrigation requirements, even under pronounced warming.

The attribution analysis (Section 3.8; Fig. 11) quantitatively supports this interpretation. Precipitation explains 74% of interannual IWU variability during the historical period and remains the dominant driver under future scenarios. However, the relative contribution of temperature increases toward the late century, particularly under RCP8.5, indicating a strengthening warming signal under intensified climate change. These findings confirm that while annual irrigation dynamics remain precipitation-controlled, temperature effects become increasingly relevant in a warmer climate.

This behavior is consistent with large-scale irrigation modeling studies. Nazemi and Wheater (2015) show that most land surface and hydrological models represent IWU as the water required to restore soil moisture toward a prescribed threshold, making IWU highly sensitive to precipitation variability. Similarly, Nie et al. (2021) report that precipitation explains most interannual irrigation variability across the contiguous United States, with temperature exerting a secondary effect. Recent studies have further emphasized that irrigation should be considered within broader land–water–climate interactions. For example, Yao et al. (2025) showed that climate change can intensify irrigation-induced land water depletion. In this regard, our catchment scale results are still in line with this broader concern: in humid monsoon basins, the direction of annual IWU change can be strongly conditioned by future precipitation changes.

4.2. Seasonal redistribution as the dominant adjustment of IWU

As shown in Fig. 6, IWU exhibits a pronounced “summer decline–autumn rise” pattern under future climate scenarios, with reduced IWU in July–August and increased IWU in October–November. Although annual irrigation totals provide an integrated measure of IWU, they do not capture the dominant mode through which climate variability influences irrigation in humid monsoon basins. This projected redistribution mainly reflects shifts in rainfall timing within the growing season and their effects on soil moisture and evapotranspiration. Thus, the annual decrease in IWU should not be interpreted as a uniform reduction in irrigation demand throughout the growing season. Instead, it masks a seasonal shift in irrigation pressure from the main monsoon period toward the late growing season.

This seasonal redistribution is further supported by the monthly changes in climate and land-surface water conditions shown in Figs. 4 and 5. Summer reductions in IWU coincide with increased precipitation during the main monsoon period and wetter soil moisture conditions in July–August, which partly compensate for warming-enhanced evapotranspiration and reduce the need for irrigation. In contrast, the increase in IWU during September–November occurs when precipitation shows a drying tendency and soil moisture declines, while evapotranspiration

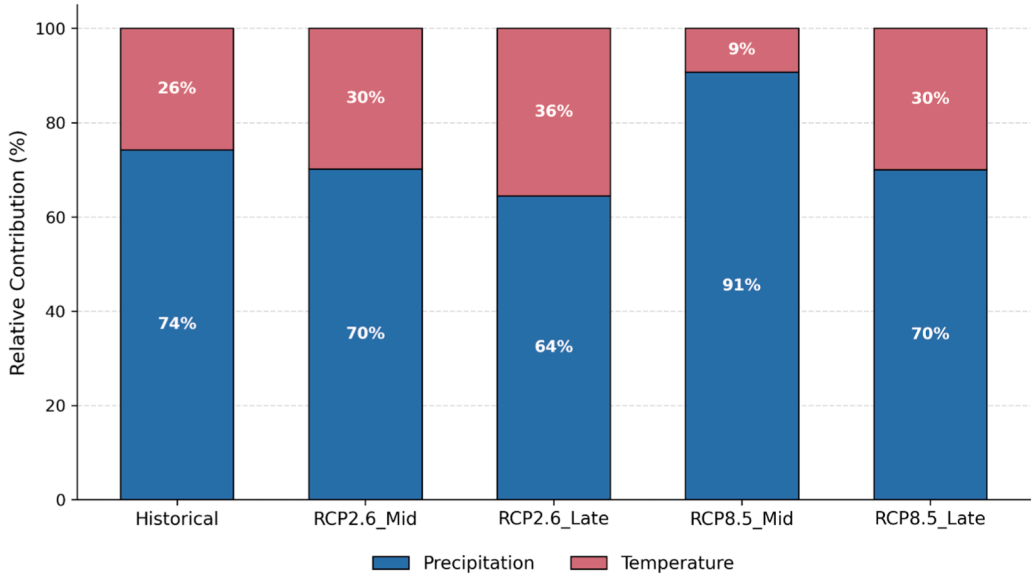

Fig. 11. Relative contributions of precipitation (blue) and temperature (pink) to variations in IWU over PLB under historical and future climate scenarios (RCP2.6 and RCP8.5).

remains elevated under warmer conditions. This mismatch causes rainfall to become insufficient to replenish the root-zone water depleted by continued evapotranspiration, thereby lowering soil moisture and triggering more frequent or larger irrigation applications in autumn. Against the background of the "wet-get-wetter and dry-get-drier" pattern reported for China (Lin et al., 2024), the seasonal redistribution identified in the PLB suggests that increased summer rainfall can suppress irrigation demand, whereas reduced autumn rainfall, combined with sustained evaporative demand, may intensify irrigation pressure during the late growing season.

Similar seasonal rainfall and growing season shifts have also been reported in historical periods (Biemans et al., 2016; Nie et al., 2021) and under future climate change conditions (Ahmad et al., 2023; Deng et al., 2025). For example, Nie et al. (2021) quantified the sensitivity of simulated irrigation water use to climate variability and found that IWU is more sensitive to precipitation variability than to temperature variability, highlighting the importance of rainfall timing in shaping seasonal irrigation responses. With respect to growing season shift, Ahmad et al. (2023) found that irrigation demand in the Indus–Ganges–Brahmaputra basins changes differently across rice growth phases, i.e., increasing during the reproductive phase but decreasing during the vegetative phase. However, because crop calendars are fixed in this study, the seasonal redistribution of IWU identified in our study mainly reflects changes in rainfall and evapotranspiration under fixed crop phenology.

We are fully aware of the increasing blue-water demand and scarcity in major breadbasket regions, including our study area (Deng et al., 2025). Their study showed that irrigation demand is strongly influenced by monthly crop water demand and seasonal water availability, particularly for specific crop types. Our process-based, multi-cropping modeling framework further demonstrates how annual irrigation totals can obscure critical seasonal variations. The seasonal redistribution of IWU identified in the PLB suggests that irrigation risk depends on both water demand and its timing relative to water availability. These findings imply that current irrigation planning and scheduling policies in the PLB need to be adapted to finer temporal scales, particularly during the late growing season (September–November), when rainfall replenishment declines but crops may still require substantial irrigation.

This result has direct implications for agricultural water management. To address the projected high temporal instability of water resources, we suggest that water allocation policies for irrigated agriculture in the PLB should be refined on finer temporal scales. Ideally, sub-seasonal to seasonal climate forecast-informed irrigation policies are recommended to support optimal agricultural water management, particularly in the PLB where irrigation stress is projected to intensify during September–November.

4.3. Crop-specific irrigation sensitivity and amplification under compound dry–hot conditions

As shown in Fig. 8, rice and non-rice irrigation exhibit distinctly different seasonal patterns. Rice irrigation dominates total IWU during the main growing season, whereas non-rice irrigation contributes a smaller annual volume but displays sharper seasonal peaks. Distinguishing between crop types is therefore essential for interpreting the heterogeneous irrigation responses identified in this study. In humid monsoon basins such as PLB, double-cropping rice systems account for the majority of irrigated area and IWU, while non-rice crops contribute less to annual total but exhibit stronger temporal variability. Treating irrigation as a crop-agnostic process would obscure these fundamentally different controls.

Rice irrigation reflects paddy water management practices that maintain near-saturated soil or shallow ponding during the growing season. Within the CDI framework, rice IWU is regulated by atmospheric demand, field-scale water balance constraints, and prescribed irrigation periods (Yang et al., 2025). Enhanced monsoon precipitation can therefore directly substitute for irrigation inputs when rainfall is sufficient. As a consequence, warming-induced increases in evapotranspiration tend to intensify intra-seasonal irrigation requirements, but precipitation compensation can offset part of this effect, producing muted or even declining total rice IWU. The rice response is mainly characterized by a redistribution within the growing season. Although total rice IWU generally decreases under future climate scenarios, its increases during the growing period become steeper, indicating that irrigation demand becomes more concentrated within key months. This suggests that both the timing and magnitude of irrigation demand should be considered when evaluating future rice irrigation risk. This behavior is consistent with previous evidence that increased rainfall can moderate annual paddy irrigation demand, while the seasonal timing of rainfall relative to peak water demand remains a critical control on irrigation requirements (Yoshino and Suppiah, 1984; Chung et al., 2011; Rhymee et al., 2024).

By contrast, non-rice irrigation responds more directly to root-zone soil moisture depletion, making it highly sensitive to the combined effects of precipitation deficits and elevated evaporative demand. In the simulations, non-rice IWU remains low during the monsoon season but concentrates into a pronounced late-monsoon peak, reflecting increased soil moisture stress as rainfall declines while atmospheric demand remains high. Similar seasonal concentration of upland-crop irrigation has been reported in monsoon-dominated regions, where rainfall during the main monsoon season substantially reduces irrigation demand but dry-season water stress intensifies irrigation requirements. For example, Biemans et al. (2016) showed that IWU is relatively low during the monsoon growing season but substantially higher during the dry-season cropping period in South Asian monsoon systems. These findings suggest that seasonal redistribution driven by rainfall seasonality can dominate irrigation responses in monsoon-influenced regions.

The contrasting responses of rice and non-rice irrigation help explain why basin-mean irrigation water use may decline even as irrigation stress intensifies during specific periods. Because rice dominates annual irrigation totals and benefits from rainfall compensation under paddy management, reductions in rice demand can lower the basin-wide annual average. Meanwhile, non-rice irrigation, though contributing less to annual totals, plays a larger role in shaping late-season peaks. Irrigation risk thus becomes increasingly concentrated in the late growing season.

This difference becomes particularly important under compound dry–hot conditions. When precipitation deficits coincide with elevated temperatures, IWU increases more sharply than under single drivers alone, consistent with compound-event theory (Zscheischler et al., 2018, 2020). Such combined amplification is likely stronger in non-rice systems that respond directly to soil moisture depletion, whereas rice responses depend on the ability to maintain ponding conditions through surface water availability.

4.4. Spatial hotspots and local controls of IWU responses

In this study, we identified local hotspots, namely, Jiujiang and Fuzhou, where IWU exhibits contrasting responses to climate change. We attribute these contrasting IWU responses primarily to differences in projected precipitation and temperature changes (Fig. S3 and S4). For example, Jiujiang is projected to experience a drier and substantially warmer future climate. Under these conditions, a warming-induced increase in evapotranspiration, together with reduced rainfall, leads to larger soil moisture deficits and consequently higher IWU. In contrast, Fuzhou is projected to become warmer but strongly wetter. The increased precipitation results in wetter soils and partly offsets the warming-enhanced evapotranspiration, thereby reducing IWU.

In addition to external forcings, land surface characteristics also modulate local IWU responses. Agronomically, Jiujiang, known as a "water-rich rice belt", is characterized by double-cropping rice systems and freshwater-based agriculture. These hydrology-dependent

agricultural systems are particularly vulnerable to climate change. In contrast, the upland agriculture in Fuzhou is generally more resilient to variations in water availability, especially under wetter future conditions. Therefore, agricultural water management strategies for these two identified hotspots should account for both external forcings and local agronomic characteristics.

These results suggest that agricultural water management in PLB should account for spatial differences in future IWU responses. To support decision making in sustainable agricultural water management, refining the indicator framework through localized agronomic analysis and stakeholder engagement could provide a new avenue for practice. In this regard, areas where IWU is projected to increase, e.g., Jiujiang, may need advanced water-saving irrigation practices, particularly for non-rice crops during warmer and drier periods. In contrast, areas where IWU is projected to decrease, such as the largest farmland region Fuzhou, may benefit more from optimizing multiple-cropping systems and irrigation scheduling strategies when sufficient irrigation water is projected to be available.

4.5. Uncertainties and limitations

In this section, we further discuss the sources of uncertainty in our irrigation modeling study, including those arising from external forcing, modeling framework, and model parameterization.

In this study, we use the RCM-based CORDEX-EA projections, because these simulations provide high-resolution, localized climate data for impact and adaptation planning through dynamical downscaling. Daily climate data during historical periods have been intensively evaluated against multiple observations across China, and the added values of RCM-based downscaling in reproducing temperature and precipitation characteristics over China have been clearly elaborated in Gu et al. (2018). Together with future projections, they have further facilitated numerous hydrological and agricultural impact studies.

For our irrigation impact study at the catchment scale, we evaluate not only CORDEX-EA Phase I outputs, but also CORDEX-EA Phase II simulations due to their higher spatial resolution (25 km). This is supported by a previous study showing that the 25-km regional climate simulations from CORDEX-EA Phase II outperform the corresponding CMIP5 GCMs and CMIP6 GCM ensembles as well, with respect to temperature, precipitation, and relative humidity (Yu et al., 2023).

Regarding the selection of climate scenarios, our NOAH-HMS-CDI simulations are currently restricted to RCP-based climate scenarios. Nevertheless, this experimental design enables us to integrate our agricultural impact assessment with previous studies on the terrestrial (Dong et al., 2019) and atmospheric (Wei et al., 2024) water cycles, thereby facilitating a more comprehensive evaluation of synergies for sustainable agricultural water management in the Poyang Lake basin. We are fully aware of the latest Shared Socioeconomic Pathways SSP-based climate scenarios, which incorporate socio-economic development pathways in addition to emissions trajectories. However, for our target region, characterized by complex terrain and a monsoon-dominated climate system, dynamically downscaled SSP simulations from regional climate models are still limited in ensemble size and may not yet adequately capture the full range of uncertainties in projected temperature and precipitation changes (Zhang et al., 2022). Therefore, in this study, we adopted RCP2.6 and RCP8.5 as representative very low- and very high-emissions scenarios respectively, as practical alternatives to SSP1–2.6 and SSP5–8.5. We expect that the findings of this study will provide useful guidance for future SSP-based irrigation impact studies in the region.

It is widely acknowledged that uncertainties may arise from the model itself (Vrugt et al., 2003), and this also applies to our modeling study. Our model sensitivity analysis of the irrigation intensification scenarios (Section 3.6) showed that intensified agricultural practices generally require higher IWU. We found that the ratio between the extent of irrigation intensification and the estimated basin-averaged IWU under RCP8.5 was approximately 0.02 under the FRA + 5% scenario and 0.05 under the FRA + 10% scenario, averaged for 30 years. This suggests that, in our target region, irrigation intensification does not result in substantial changes in water resource allocation to the agricultural sector under high-emission warming scenarios. In other words, on the catchment scale, it is possible to implement intensive agriculture there and achieve the sustainable development goal of food security in a warming condition.

We also acknowledge that hard-coded parameters and simplified processes in the NOAH-HMS-CDI modeling framework could impact the estimated IWU. For our irrigation impact assessment, the crop-specific irrigation scheme proposed in Yang et al. (2025) has been applied. It is expected that different irrigation-triggering thresholds, target water conditions, or irrigation periods affect the magnitude and seasonal distribution of the simulated IWU. However, the decision was taken to utilize the same irrigation scheme, incorporating time-invariant lower boundary conditions for land-use and crop information in this instance. This modeling strategy is adopted to ensure consistent agricultural background conditions between historical and future simulations, thereby facilitating more precise isolation of the climate-driven IWU response. Future work could incorporate dynamic phenology, land-use, and cropping-pattern scenarios to further assess how agricultural structural changes interact with climate change in shaping future IWU.

5. Conclusions

This study applied the NOAH-HMS-CDI land surface–hydrological model to project future irrigation water use in PLB under climate change. The model explicitly represents crop-specific irrigation processes for rice and non-rice crops. Despite projected warming and increased evapotranspiration, basin-mean IWU generally decreases in most scenarios, mainly because increased precipitation compensates for part of the warming-induced water demand. However, this basin-mean decline does not capture pronounced temporal and spatial heterogeneity.

Future IWU shows a clear seasonal redistribution, with reduced IWU in mid-summer and increased IWU during September–November under projected autumn drying. Rice and non-rice crops respond differently to these changes. Rice IWU generally decreases because rainfall can partly substitute for irrigation in paddy fields, although the within-season rise in rice irrigation becomes steeper. Non-rice irrigation shows greater interannual variability and stronger sensitivity to late-season drying than rice irrigation. Spatially, warming-dominated areas such as Jiujiang show increasing IWU and emerge as local hotspots, while precipitation-enhanced areas such as Fuzhou experience declining IWU. Dry–Hot years are generally associated with higher IWU than wetter conditions, indicating that compound dry-hot conditions can increase short-term irrigation pressure. Precipitation remains the dominant driver of interannual IWU variability, while the influence of temperature strengthens toward the late century.

These findings have direct implications for agricultural water management in PLB. Irrigation planning should extend the critical supply period into autumn, especially September–November. Region-specific allocation strategies are also needed. Hotspot areas may require stronger water-supply regulation and infrastructure support, while wetter sub-regions may benefit more from improving effective rainfall use and field-level water management. In addition, Dry–Hot years should be treated as warning conditions because they can create short-term pressure on irrigation supply.

Overall, future irrigation risk in humid monsoon basins is shaped not only by changes in annual water demand but also by seasonal redistribution, crop-specific responses, spatial hotspots, and compound dry–hot conditions. These process-based projections provide a scientific basis for climate-resilient irrigation planning and agricultural water management under ongoing climate change.

CRediT authorship contribution statement

Jianyong Ma: Writing – review & editing, Software, Methodology. **Huanghe Gu:** Software, Resources, Methodology, Data curation. **Chuanguo Yang:** Software, Resources, Methodology, Data curation. **Jianhui Wei:** Writing – review & editing, Writing – original draft, Supervision, Software, Methodology. **Qianya Yang:** Writing – review & editing, Writing – original draft, Visualization, Validation, Software, Resources, Project administration, Methodology, Investigation, Funding acquisition, Formal analysis, Data curation, Conceptualization. **Zhongbo Yu:** Supervision. **Lifeng Wu:** Writing – review & editing. **Ningpeng Dong:** Methodology, Data curation.

Declaration of Competing Interest

The authors declare that they have no known competing financial interests or personal relationships that could have appeared to influence the work reported in this paper.

Acknowledgements

This work was financially supported by Jiangxi Provincial Natural Science Foundation (20224BAB214080), the Belt and Road Special Foundation of the National Key Laboratory of Water Disaster Prevention (2022490111), the National Natural Science Foundation of China (U2240217, 42271020, U25A20752), and the German Research Foundation (DFG) through funding of the AccHydro project (KU 2090/11–1).

Appendix A. Supporting information

Supplementary data associated with this article can be found in the online version at doi:10.1016/j.agwat.2026.110538.

Data availability

Data will be made available on request.

References

Acharjee, T.K., Ludwig, F., van Halsema, G., Hellegers, P., Supit, I., 2017. Future changes in water requirements of Boro rice in the face of climate change in North-West Bangladesh. Agric. Water Manag. 194. https://doi.org/10.1016/j.agwat.2017.09.008.

Ahmad, Q.-A., Moors, E., Biemans, H., Shaheen, N., Masih, I., ur Rahman Hashmi, M.Z., 2023. Climate-induced shifts in irrigation water demand and supply during sensitive crop growth phases in South Asia. Clim. Change 176 (11), 150. https://doi.org/10.1007/s10584-023-03629-7.

Bao, Y., Gao, Y., Lü, S., Wang, Q., Zhang, S., Xu, J., Li, R., Li, S., Ma, D., Meng, X., Chen, H., Chang, Y., 2014. Evaluation of CMIP5 earth system models in reproducing leaf area index and vegetation cover over the tibetan plateau. J. Meteorol. Res. 28 (6). https://doi.org/10.1007/s13351-014-4023-5.

Biemans, H., Siderius, C., Mishra, A., Ahmad, B., 2016. Crop-specific seasonal estimates of irrigation-water demand in South Asia. Hydrol. Earth Syst. Sci. 20 (5). https://doi.org/10.5194/hess-20-1971-2016.

Chen, F., Dudhia, J., 2001. Coupling an advanced land surface-hydrology model with the Penn State-NCAR MM5 modeling system. Part I: Model implementation and sensitivity. Mon. Weather. Rev. https://doi.org/10.1175/1520-0493(2001)129<0569:CAALSH>2.0.CO;2.

Chen, X., Yu, Z., Yi, P., Aldahan, A., Hwang, H.-T., Sudicky, E.A., 2023. Disentangling runoff generation mechanisms: Combining isotope tracing with integrated surface/subsurface simulation. J. Hydrol. 617, 129149. https://doi.org/10.1016/j.jhydrol.2023.129149.

Chen, X., Yu, Z., Yi, P., Chen, P., Hwang, H.-T., Sudicky, E.A., Simonovic, S.P., 2024. Water sources and threshold behaviors of streamflow generation in a headwater catchment revealed by hydrological modeling and isotopic tracing. J. Hydrol. 644, 132117. https://doi.org/10.1016/j.jhydrol.2024.132117.

Chung, S.O., Rodríguez-Díaz, J.A., Weatherhead, E.K., Knox, J.W., 2011. Climate change impacts on water for irrigating paddy rice in South Korea. Irrig. Drain. 60 (2). https://doi.org/10.1002/ird.559.

De Silva, C.S., Weatherhead, E.K., Knox, J.W., Rodriguez-Diaz, J.A., 2007. Predicting the impacts of climate change-A case study of paddy irrigation water requirements in Sri Lanka. Agric. Water Manag. 93 (1–2), 19–29. https://doi.org/10.1016/j.agwat.2007.06.003.

Deng, Q., Sharretts, T., Ali, T., Ao, Y.Z., Chiarelli, D.D., Demeke, B., Marston, L., Mehta, P., Mekonnen, M., Rulli, M.C., Tuninetti, M., Xie, W., Davis, K.F., 2025. Deepening water scarcity in breadbasket nations. Nat. Commun. 16 (1), 1110. https://doi.org/10.1038/s41467-025-56022-6.

Döll, P., Siebert, S., 2002. Global modeling of irrigation water requirements, 8-1-8–10 Water Resour. Res. 38 (4). https://doi.org/10.1029/2001wr000355.

Dong, G., Jiang, Z., Tian, Z., Buonomo, E., Sun, L., Fan, D., 2020. Projecting Changes in Mean and Extreme Precipitation Over Eastern China During 2041–2060. Earth Space Sci. 7 (9). https://doi.org/10.1029/2019EA001024.

Dong, N., Wei, J., Yang, M., Yan, D., Yang, C., Gao, H., et al., 2022. Model estimates of China's terrestrial water storage variation due to reservoir operation. Water Resour. Res. 58, e2021WR031787. https://doi.org/10.1029/2021WR031787.

Dong, N., Yu, Z., Gu, H., Yang, C., Yang, M., Wei, J., Wang, H., Arnault, J., Laux, P., Kunstmann, H., 2019. Climate-induced hydrological impact mitigated by a high-density reservoir network in the Poyang Lake Basin. J. Hydrol. 579. https://doi.org/10.1016/j.jhydrol.2019.124148.

Elgaali, E., Garcia, L.A., Ojima, D.S., 2007. High resolution modeling of the regional impacts of climate change on irrigation water demand. Clim. Change. https://doi.org/10.1007/s10584-007-9278-8.

Fischer, G., Tubiello, F.N., van Velthuizen, H., Wiberg, D.A., 2007. Climate change impacts on irrigation water requirements: Effects of mitigation, 1990-2080. Technol. Forecast. Soc. Change. https://doi.org/10.1016/j.techfore.2006.05.021.

Frederick, K.D., Major, D.C., 1997. Climate change and water resources. Clim. Change 37, 7–23. https://doi.org/10.1023/A:1005336924908.

Gu, H., Yu, Z., Yang, C., Ju, Q., Yang, T., Zhang, D., 2018. High-resolution ensemble projections and uncertainty assessment of regional climate change over China in CORDEX East Asia. Hydrol. Earth Syst. Sci. 22 (5). https://doi.org/10.5194/hess-22-3087-2018.

Haile, G.G., Tang, Q., Reda, K.W., Baniya, B., He, L., Wang, Y., Gebrechorkos, S.H., 2024. Projected impacts of climate change on global irrigation water withdrawals. Agric. Water Manag. 305, 109144. https://doi.org/10.1016/j.agwat.2024.109144.

Hanasaki, N., Fujimori, S., Yamamoto, T., Yoshikawa, S., Masaki, Y., Hijioka, Y., Kainuma, M., Kanamori, Y., Masui, T., Takahashi, K., Kanae, S., 2013. A global water scarcity assessment under Shared Socio-economic Pathways - Part 2: Water availability and scarcity. Hydrol. Earth Syst. Sci. 17 (7). https://doi.org/10.5194/hess-17-2393-2013.

Hao, H., Dong, N., Yang, M., Wei, J., Zhang, X., Xu, S., et al., 2024. The changing hydrology of an irrigated and dammed Yangtze River: Streamflow, extremes, and lake hydrodynamics. Water Resour. Res. 60, e2024WR037841. https://doi.org/10.1029/2024WR037841.

Hu, B., Tang, J., Ding, J., Liu, G., 2021. Regional downscaled future change of clear-air turbulence over East Asia under RCP8.5 scenario within the CORDEX-EA-II project. Int. J. Climatol. 41 (10). https://doi.org/10.1002/joc.7114.

Jägermeyr, J., Pastor, A., Biemans, H., Gerten, D., 2017. Reconciling irrigated food production with environmental flows for Sustainable Development Goals implementation. Nat. Commun. 8 (1), 15900. https://doi.org/10.1038/ncomms15900.

Jin, C.S., Cha, D.H., Lee, D.K., Suh, M.S., Hong, S.Y., Kang, H.S., Ho, C.H., 2016. Evaluation of climatological tropical cyclone activity over the western North Pacific in the CORDEX-East Asia multi-RCM simulations. Clim. Dyn. 47 (3–4). https://doi.org/10.1007/s00382-015-2869-6.

Lee, J.Y., Wang, B., 2014. Future change of global monsoon in the CMIP5. Clim. Dyn. 42 (1–2). https://doi.org/10.1007/s00382-012-1564-0.

Leng, G., Huang, M., Tang, Q., Sacks, W.J., Lei, H., Leung, L.R., 2013. Modeling the effects of irrigation on land surface fluxes and states over the conterminous United States: Sensitivity to input data and model parameters. J. Geophys. Res. Atmospheres 118 (17), 9789–9803. https://doi.org/10.1002/jgrd.50792.

Leng, G., Tang, Q., 2014. Modeling the impacts of future climate change on irrigation over China: Sensitivity to adjusted projections. J. Hydrometeorol. 15 (5), 2085–2103. https://doi.org/10.1175/JHM-D-13-0182.1.

Lin, S., Sun, X., Huang, K., Song, C., Sun, J., Sun, S., Wang, G., Hu, Z., 2024. The seasonal variability of future evapotranspiration over China during the 21st century. Sci. Total Environ. 926. https://doi.org/10.1016/j.scitotenv.2024.171816.

Liu, F., Guan, S., Deng, H., Li, X., Cai, S., 2019. Study on Rice Irrigation Quota at Different Regional Scales in Typical Irrigated Areas of Poyang Lake Basin. Water Sav. Irrig. 04, 12–15 (in Chinese).

Mehta, P., Siebert, S., Kummu, M., Deng, Q., Ali, T., Marston, L., Xie, W., Davis, K.F., 2024. Half of twenty-first century global irrigation expansion has been in water-stressed regions. Nat. Water 2 (3), 254–261. https://doi.org/10.1038/s44221-024-00206-9.

Monfreda, C., Ramankutty, N., Foley, J.A., 2008. Farming the planet: 2. Geographic distribution of crop areas, yields, physiological types, and net primary production in the year 2000. Glob. Biogeochem. Cycles 22 (1). https://doi.org/10.1029/2007GB002947.

Nazemi, A., Wheater, H.S., 2015. On inclusion of water resource management in Earth system models -Part 1: Problem definition and representation of water demand. Hydrol. Earth Syst. Sci. https://doi.org/10.5194/hess-19-33-2015.

Nie, W., Zaitchik, B.F., Rodell, M., Kumar, S.V., Arsenault, K.R., Badr, H.S., 2021. Irrigation Water Demand Sensitivity to Climate Variability Across the Contiguous United States. Water Resour. Res. 57 (3). https://doi.org/10.1029/2020WR027738.

Park, J.H., Oh, S.G., Suh, M.S., 2013. Impacts of boundary conditions on the precipitation simulation of RegCM4 in the CORDEX East Asia domain. J. Geophys. Res. Atmospheres 118 (4). https://doi.org/10.1002/jgrd.50159.

Rhymee, H., Shams, S., Ratnayake, U., Rahman, E.K.A., 2024. Projecting Irrigation Water and Crop Water Requirements for Paddies Using WEAP-MABIA under Climate Change. Water (Switz.) 16 (17). https://doi.org/10.3390/w16172498.

Rosa, L., Chiarelli, D.D., Sangiorgio, M., Beltran-Peña, A.A., Rulli, M.C., D'Odorico, P., Fung, I., 2020. Potential for sustainable irrigation expansion in a 3 °C warmer climate. Proc. Natl. Acad. Sci. 117 (47), 29526–29534. https://doi.org/10.1073/pnas.2017796117.

Santikayasa, I.P., Babel, M.S., Shrestha, S., Jourdain, D., Clemente, R.S., 2014. Evaluation of water use sustainability under future climate and irrigation management scenarios in Citarum River Basin, Indonesia. Int. J. Sustain. Dev. World Ecol. 21 (2). https://doi.org/10.1080/13504509.2014.884023.

Schlenker, W., Hanemann, W.M., Fisher, A.C., 2007. Water availability, degree days, and the potential impact of climate change on irrigated agriculture in California. Clim. Change 81 (1). https://doi.org/10.1007/s10584-005-9008-z.

Shah, W.U.H., Hao, G., Yasmeen, R., Yan, H., Shen, J., Lu, Y., 2023. Role of China's agricultural water policy reforms and production technology heterogeneity on agriculture water usage efficiency and total factor productivity change. Agric. Water Manag. 287, 108429. https://doi.org/10.1016/j.agwat.2023.108429.

Shen, W., Tang, J., Wang, Y., Wang, S., Niu, X., 2017. Evaluation of WRF model simulations of tropical cyclones in the western North Pacific over the CORDEX East Asia domain. Clim. Dyn. 48 (7–8). https://doi.org/10.1007/s00382-016-3213-5.

Siew, J.H., Tangang, F.T., Juneng, L., 2014. Evaluation of CMIP5 coupled atmosphere-ocean general circulation models and projection of the Southeast Asian winter monsoon in the 21st century. Int. J. Climatol. 34 (9). https://doi.org/10.1002/joc.3880.

Skamarock, W.C., et al., 2008. A description of the advanced research WRF version 3, NCAR Tech. Note, NCAR/TN-468+STR. Natl. Cent. Atmos. Res. Boulder Colo. https://doi.org/10.5065/D68S4MVH.

Sun, S.K., Li, C., Wu, P.T., Zhao, X.N., Wang, Y.B., 2018. Evaluation of agricultural water demand under future climate change scenarios in the Loess Plateau of Northern Shaanxi, China. Ecol. Indic. 84. https://doi.org/10.1016/j.ecolind.2017.09.048.

Tang, J., Wang, S., Niu, X., Hui, P., Zong, P., Wang, X., 2017. Impact of spectral nudging on regional climate simulation over CORDEX East Asia using WRF. Clim. Dyn. 48 (7–8). https://doi.org/10.1007/s00382-016-3208-2.

Thomas, A., 2008. Agricultural irrigation demand under present and future climate scenarios in China. Glob. Planet. Change 60 (3–4). https://doi.org/10.1016/j.gloplacha.2007.03.009.

Tukimat, N.N.A., Harun, S., Shahid, S., 2017. Modeling Irrigation Water Demand in a Tropical Paddy Cultivated Area in the Context of Climate Change. J. Water Resour. Plan. Manag. 143 (7). https://doi.org/10.1061/(asce)wr.1943-5452.0000753.

Uniyal, B., Dietrich, J., 2021. Simulation of irrigation demand and control in catchments – a review of methods and case studies. Water Resour. Res. 57 (7). https://doi.org/10.1029/2020WR029263.

Vrugt, J.A., Gupta, H.V., Bouten, W., Sorooshian, S., 2003. A Shuffled Complex Evolution Metropolis algorithm for optimization and uncertainty assessment of hydrologic model parameters. Water Resour. Res. 39 (8). https://doi.org/10.1029/2002WR001642.

Wada, Y., Wisser, D., Eisner, S., Flörke, M., Gerten, D., Haddeland, I., Hanasaki, N., Masaki, Y., Portmann, F.T., Stacke, T., Tessler, Z., Schewe, J., 2013. Multimodel projections and uncertainties of irrigation water demand under climate change. Geophys. Res. Lett. 40 (17). https://doi.org/10.1002/grl.50686.

Wagner, S., Fersch, B., Yuan, F., Yu, Z., Kunstmann, H., 2016. Fully coupled atmospheric-hydrological modeling at regional and long-term scales: Development, application, and analysis of WRF-HMS. Water Resour. Res. 52 (4), 3187–3211. https://doi.org/10.1002/2015WR018185.

Wang, Y., Jiang, Z., Chen, W., 2015. Performance of CMIP5 models in the simulation of climate characteristics of synoptic patterns over East Asia. J. Meteorol. Res. 29 (4). https://doi.org/10.1007/s13351-015-4129-4.

Wang, X., Shi, W., Yu, Q., Deng, X., Zuo, L., Shi, X., Wang, M., Li, J., 2025. Well-facilitated farmland improves nitrogen use efficiency and reduces environmental impacts in the Huang-Huai-Hai Region, China. J. Integr. Agric. 24 (8), 3264–3281. https://doi.org/10.1016/j.jia.2025.02.006.

Wang, P., Tang, J., Sun, X., Liu, J., Juan, F., 2019. Spatiotemporal characteristics of heat waves over China in regional climate simulations within the CORDEX-EA project. Clim. Dyn. 52 (1–2). https://doi.org/10.1007/s00382-018-4167-6.

Wei, J., Arnault, J., Rummler, T., Fersch, B., Zhang, Z., Olschewski, P., Laux, P., Dong, N., Yang, Q., Xing, Z., Li, X., Yang, C., Zhang, X., Ma, M., Gao, L., Xu, L., Yu, Z., Kunstmann, H., 2024. Acceleration of the hydrological cycle under global warming for the poyang lake basin in southeast china: an age-weighted regional water tagging approach. J. Hydrometeorol. 25 (11), 1627–1647. https://doi.org/10.1175/JHM-D-23-0227.1.

Wei, J., Dong, N., Fersch, B., Arnault, J., Wagner, S., Laux, P., Zhang, Z., Yang, Q., Yang, C., Shang, S., Gao, L., Yu, Z., Kunstmann, H., 2021. Role of reservoir regulation and groundwater feedback in a simulated ground-soil-vegetation continuum: A long-term regional scale analysis. Hydrol. Process. 35 (8). https://doi.org/10.1002/hyp.14341.

Wisser, D., Fekete, B.M., Vörösmarty, C.J., Schumann, A.H., 2010. Reconstructing 20th century global hydrography: A contribution to the Global Terrestrial Network-Hydrology (GTN-H). Hydrol. Earth Syst. Sci. 14 (1), 1–24. https://doi.org/10.5194/hess-14-1-2010.

Wu, J., Chen, X., Lu, J., 2022. Assessment of long and short-term flood risk using the multi-criteria analysis model with the AHP-Entropy method in Poyang Lake basin. Int. J. Disaster Risk Reduct. 75. https://doi.org/10.1016/j.ijdrr.2022.102968.

Xing, Z., Wei, J., Li, Y., Zhang, X., Ma, M., Yi, P., Ju, Q., Laux, P., Kunstmann, H., 2024. Disentangling the spatially combined and temporally lagged influences of climate oscillations on seasonal droughts in the East Asian monsoon influenced Poyang Lake Basin. Atmos. Res. 310, 107603. https://doi.org/10.1016/j.atmosres.2024.107603.

Xing, Z., Yu, Z., Wei, J., Zhang, X., Ma, M., Yi, P., Ju, Q., Wang, J., Laux, P., Kunstmann, H., 2022. Lagged influence of ENSO regimes on droughts over the Poyang Lake basin, China. Atmos. Res. 275. https://doi.org/10.1016/j.atmosres.2022.106218.

Xu, J., Gao, Y., Chen, D., Xiao, L., Ou, T., 2017. Evaluation of global climate models for downscaling applications centred over the Tibetan Plateau. Int. J. Climatol. 37 (2). https://doi.org/10.1002/joc.4731.

Yang, Q., Wei, J., Yang, C., Gu, H., Ma, J., Dong, N., Arnault, J., Laux, P., Fersch, B., Shang, S., Yu, Z., Kunstmann, H., 2025. A crop-specific dynamic irrigation scheme in a regional land surface-hydrologic modeling framework for improving human water-use estimation and irrigation impact assessment. J. Hydrol. 659. https://doi.org/10.1016/j.jhydrol.2025.133322.

Yao, Y., Thiery, W., Ducharne, A., Cook, B.I., Ding, A., De Hertog, S.J., Sieber, P., Aas, K. S., Arboleda-Obando, P.F., Colin, J., Costantini, M., Decharme, B., Lawrence, D.M., Lawrence, P., Leung, L.R., Lo, M.-H., Devaraju, N., Wu, R.-J., Zhou, T., Seneviratne, S.I., 2025. Irrigation-induced land water depletion aggravated by climate change. Nat. Water 3 (12), 1424–1435. https://doi.org/10.1038/s44221-025-00529-1.

Yoo, S.H., Choi, J.Y., Nam, W.H., Hong, E., 2012. Analysis of design water requirement of paddy rice using frequency analysis affected by climate change in South Korea. Agric. Water Manag. 112. https://doi.org/10.1016/j.agwat.2012.06.002.

Yoshino, M.M., Suppiah, R., 1984. Rainfall and Paddy Production in Sri Lanka. J. Agric. Meteorol. 40 (1). https://doi.org/10.2480/agrmet.40.9.

Yu, E., Liu, D., Yang, J., Sun, J., Yu, L., King, M.P., 2023. Future climate change for major agricultural zones in China as projected by CORDEX-EA-II, CMIP5 and CMIP6 ensembles. Atmos. Res. 288, 106731. https://doi.org/10.1016/j.atmosres.2023.106731.

Yu, Z., Pollard, D., Cheng, L., 2006. On continental-scale hydrologic simulations with a coupled hydrologic model. J. Hydrol. https://doi.org/10.1016/j.jhydrol.2006.05.021.

Yu, E., Sun, J., Chen, H., Xiang, W., 2015. Evaluation of a high-resolution historical simulation over China: climatology and extremes. Clim. Dyn. 45 (7–8). https://doi.org/10.1007/s00382-014-2452-6.

Zhang, Q., Liu, Y., Yang, G., Zhang, Z., 2011. Precipitation and hydrological variations and related associations with large-scale circulation in the Poyang Lake basin, China. Hydrol. Process. 25 (5). https://doi.org/10.1002/hyp.7863.

Zhang, M., Xu, W., Hu, Z., Merz, C., Ma, M., Wei, J., Guan, X., Jiang, L., Bao, R., Wei, Y., Gao, L., 2022. Projection of future climate change in the Poyang Lake Basin of China under the global warming of 1.5–3°C. Front. Environ. Sci. 10, 2022. https://doi.org/10.3389/fenvs.2022.985145.

Zscheischler, J., Martius, O., Westra, S., Bevacqua, E., Raymond, C., Horton, R.M., van den Hurk, B., AghaKouchak, A., Jézéquel, A., Mahecha, M.D., Maraun, D., Ramos, A. M., Ridder, N.N., Thiery, W., Vignotto, E., 2020. A typology of compound weather and climate events. Nat. Rev. Earth Environ. 1 (Number 7). https://doi.org/10.1038/s43017-020-0060-z.

Zscheischler, J., Westra, S., Van Den Hurk, B.J.J.M., Seneviratne, S.I., Ward, P.J., Pitman, A., Aghakouchak, A., Bresch, D.N., Leonard, M., Wahl, T., Zhang, X., 2018. Future climate risk from compound events. Nat. Clim. Change 8 (Number 6). https://doi.org/10.1038/s41558-018-0156-3.